ARMY RESEARCH LABORATORY

The Effect of Nose Shape on Depleted Uranium (DU) Long-Rod Penetrators

by Wendy Leonard

ARL-TR-1505 September 1997

The findings in this report are not to be construed as an official Department of the Army position unless so designated by other authorized documents.

Citation of manufacturer's or trade names does not constitute an official endorsement or approval of the use thereof.

Destroy this report when it is no longer needed. Do not return it to the originator.

Army Research Laboratory
Aberdeen Proving Ground, MD 21005-5066

ARL-TR-1505 **September 1997**

The Effect of Nose Shape on Depleted Uranium (DU) Long-Rod Penetrators

Wendy Leonard
Weapons and Materials Research Directorate, ARL

Abstract

The ballistic performance of model scale U-3/4%Ti long-rod penetrators with three different nose-shape designs (blunt nose, conical nose, and frustum cone) were evaluated. The target matrix included semi-infinite rolled homogeneous armor (RHA) and two finite RHA targets, one at normal incidence and one at high obliquity, but with the same line-of-sight thickness. The results reflected the same trends as observed for a previous tungsten alloy penetrator study, demonstrating that the nose-shape effects are independent of penetrator material.

Acknowledgments

Dr. Lee Magness and Mr. Tim Farrand are acknowledged for their guidance during the planning and execution of the test series. The author would also like to recognize Mrs. Eleanor Deal (Experimental Facility Manager), Mr. Bernard McKay, Mr. Jack Koontz, Mr. Maurice Clark, Mr. Vaughn Torbert, and Mr. Richard English, the U.S. Army Research Laboratory (ARL) Experimental Facility 110 technicians who performed the actual testing.

INTENTIONALLY LEFT BLANK.

Table of Contents

INTENTIONALLY LEFT BLANK.

List of Figures

List of Tables

INTENTIONALLY LEFT BLANK.

1. Introduction

Kinetic energy (KE) penetrators have long been used as the primary munition for the U.S. Army main battle tank. As a result, many research dollars have been expended to understand the principles that make a good projectile. Studies have been done to examine penetrator materials and mechanical properties, as well as overall optimum physical characteristics, such as length-to-diameter (L/D) ratio, fin design, and nose-shape design (Zukas et al. 1992). A previous study examined the influence of nose shape on the performance of model scale tungsten heavy alloy (WHA) long-rod penetrators interacting with single plate metallic targets (Zook 1984, 1985). It concluded that, for WHA penetrators, a conical-nose-shape design performed better against a target at 0° obliquity than for a target with the same line-of-sight thickness at a high obliquity. It was also found that the inverse was true for the other nose shapes (short frustum, hemispheric, and blunt nose) tested.

Since the mid-1970s, however, the U-3/4% Ti alloy has been the material of choice for fielded KE tank round ammunition, due to its superior ballistic performance. The difference in terminal ballistic performance between the materials is rooted in a fundamental difference in the deformation and failure behaviors exhibited by the uranium and the tungsten alloys during the penetration process (Magness and Farrand 1990). Large mushroomed heads are routinely observed on residual penetrators of conventional WHAs, whereas recovered residual uranium alloy penetrators always lack this mushroomed head and, instead, have a chiseled head. Metallographic examinations reveal that early localized adiabatic shear failures occur in the uranium alloys, preventing the large bulk plastic deformation that results in the large mushroomed head observed on WHAs.

This study was conducted to determine the effect of nose shape on the performance of U-3/4% Ti penetrators against rolled homogeneous armor (RHA). It was speculated that, due to the differences in penetrator material flow and deformation characteristics, a penetrator that exhibits early shear failures may not show as much dependence on nose-shape design.

2. Projectile Characteristics

The penetrators used in this evaluation were manufactured from M-833 specification U-3/4% Ti, which has a density of 18.6 g/cm^3 and a Rockwell C hardness of approximately 40.5. Due to the higher density of the U-3/4% Ti rods, the dimensions of the final penetrators are different than the 91% W-6.3% Ni-2.7% Fe penetrators used in the earlier study (density = 17.3 g/cm^3) for the same L/D geometry. Each of the U-3/4% Ti penetrators had a L/D ratio of 10 with a diameter of 7.70 mm and a nominal mass of 66 g. All of the rods were right circular cylinders with nose shapes selected from the two extremes and also the midperformer of the WHA penetrator designs tested by Zook. The chosen nose shapes included a blunt nose, a frustum cone that was truncated at 0.6 of the diameter, and a full cone with a total apex angle of 15.5°. Similar to the test series with the WHA nose-shape projectiles, the lengths of the cylindrical portion of the rods were adjusted so that the mass and diameter remained constant for the three nose-shape designs. This eliminated the need to correct for effective length when comparing terminal ballistic performance. Figures 1 and 2 illustrate the dimensions of each of the chosen penetrator designs for the U-3/4% Ti and WHA penetrators, respectively.

3. Target Matrix

The test matrix included both semi-infinite and finite monolithic RHA targets. Semi-infinite targets are those where penetration is not influenced by free surface effects (from the side or rear). This type of test examines the actual penetration capability of the rod. Finite targets, on the other hand, are used to quantify perforation capabilities. The finite targets selected, a 76.2-mm RHA plate at 0° obliquity and a 25.4-mm RHA plate at 70.5° obliquity, have the same line-of-sight thickness. To eliminate any variability in performance due to target hardness, the 25.4-mm RHA plate was heat-treated to the same hardness as the 76.2-mm RHA plate (Brinell hardness number [BHN] = 269–286). The BHN of each of the target plates was checked prior to testing to guarantee the correct target hardness.

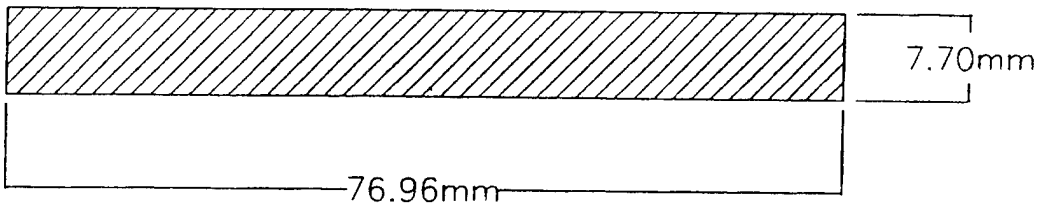

(a) Blunt-Nose-Design Penetrator.

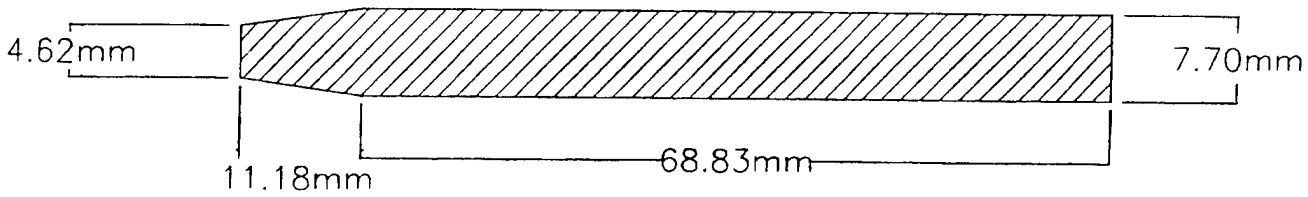

(b) Frustum-Nose-Design Penetrator.

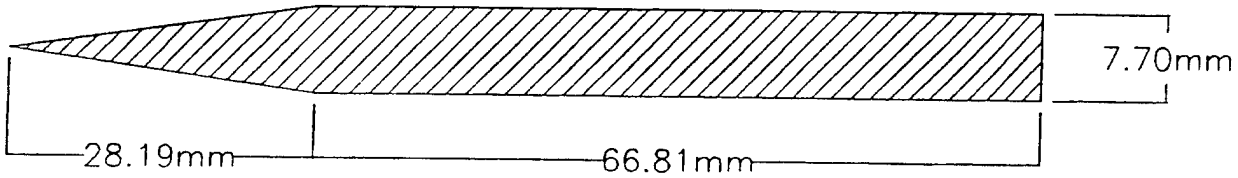

(c) Conical-Nose-Design Penetrator.

Figure 1. Dimensions and Geometries of the U-3/4% Ti Nose-Shape Projectiles.

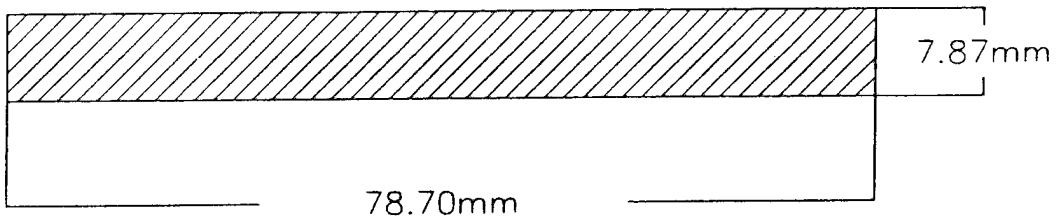

(a) Blunt-Nose-Design Penetrator.

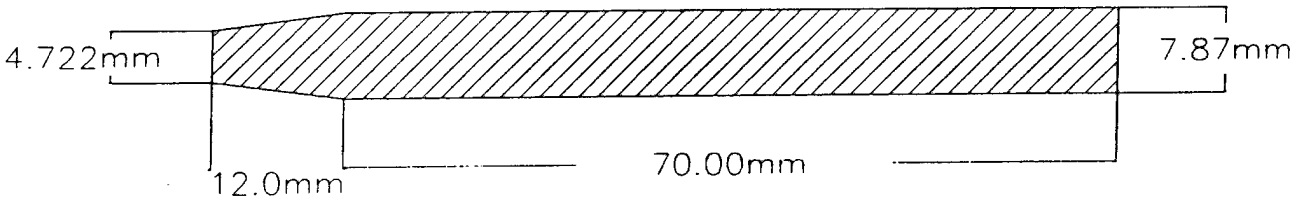

(b) Frustum-Nose-Design Penetrator.

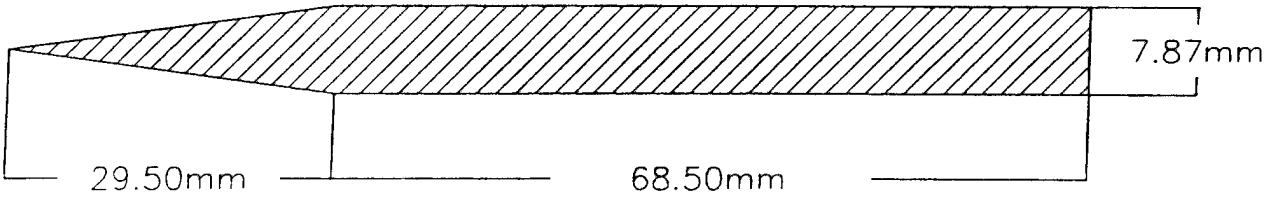

(c) Conical-Nose-Design Penetrator.

Figure 2. Dimensions and Geometries of the WHA Nose-Shape Projectiles.

4. Test Procedure

Testing was conducted using an approximate 26-mm-diameter smoothbore laboratory gun system at the U.S. Army Research Laboratory's (ARL's) Experimental Facility 110. Each penetrator was supported in the barrel during launch by a polypropulux sabot, a four-piece design with a concave front-end design that helps separate the petals after exiting the gun. This quick discard of the sabot does not interfere with the penetrator/target interaction. Following the sabot is a steel pusher plate embedded in a polypropulux obturator. The pusher plate distributes the launch forces over a wider area, thereby preventing the rod from setting back into the soft plastic obturator. The back end of the obturator is machined to a slightly larger outer diameter than the sabot to seal the propellant gases behind the launch package, which accelerates the package to the required velocity. The short distance from the muzzle of the gun to the target of about 3 m helped to ensure acceptable yaw values upon impact.

Two pairs of orthogonal x-ray tube stations, located in front of the target, record images of the penetrator prior to target impact. Preimpact conditions of the projectile, such as pitch, yaw, and velocity, are determined from these radiographs (Grabarek and Herr 1966). For finite thickness plate tests, an additional pair of tube heads is placed behind the target, solely in the vertical plane, to capture images of the residual penetrator and behind-armor debris exiting the target. Residual velocities, masses, and flight characteristics are calculated using these images. A schematic of the range and x-ray setup is presented in Figure 3.

Terminal ballistic evaluations typically begin by determining the depth of penetration into semi-infinite armor. A semi-infinite target is of sufficient thickness and width so that the penetration event is not influenced by any free-surface effects, and the test solely examines the penetration capabilities of the rod. Cubes of 152-mm RHA, with BHN hardness of 255–269, were fired into at velocities of 900 m/s to 1,500 m/s in 200-m/s increments. These targets were later sectioned down the midline of the penetration channel, and the final penetration depths were measured.

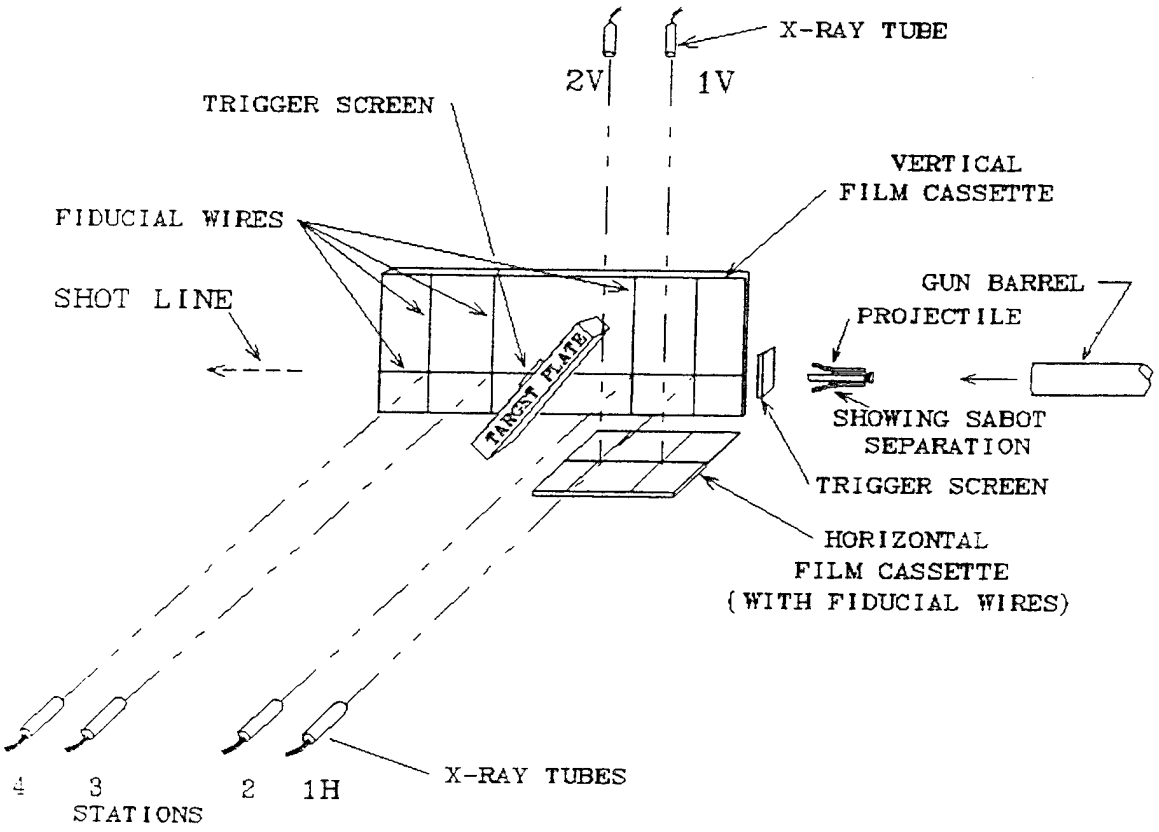

Figure 3. Schematic of the Range and X-ray Setup.

Once the semi-infinite performance is quantified, limit velocities into finite targets are determined. A limit velocity is the velocity at which a penetrator will just perforate a target with a residual velocity of zero. Each limit velocity is calculated using a least-squares fit of the Lambert-Jonas (1976) equation to the striking velocity and residual velocity data pairs (Vs, Vr) measured from the radiographs. Approximately six shots were fired for each limit velocity determination. These tests provide additional insight into the capabilities of the penetrator nose-shape designs, since they involve both the penetration and perforation phases.

All of the preimpact, in-flight, and postimpact parameters recorded in each test are described in Appendix A. For each of the shots, various target measurements, including entrance/exit hole size, depth of penetration, bulge characteristics, and center hole dimensions, are listed in Appendix B. When appropriate, limit velocity curves are included with the finite target data.

5. Ballistic Test Results

The results of the effectively semi-infinite RHA target tests at normal incidence are given in Table 1. These data points are also graphically represented in Figure 4, a plot of U-3/4% Ti nose-shape, rod-penetration data as a function of impact velocity. At all velocities, the conical-nose-shape penetrator, the longest projectile design, is the best performer against these normal-incidence targets. The second best performer is the frustum cone, and the worst performer is the blunt-nose penetrator design, the shortest of these penetrator designs.

Table 1. Semi-Infinite Results at Normal Incidence

Nose Shape	Striking Velocity (m/s)	Penetration (mm)
Blunt	941	34.9
	1,046	43.8
	1,252	62.9
	1,492	83.2
Frustum Cone	924	31.1
	1,070	47.6
	1,331	71.8
	1,493	85.7
Conical	915	43.8
	1,101	60.3
	1,299	79.4
	1,505	103.5

A vastly different effect is seen in Figure 5, a plot of normalized penetration as a function of velocity, as compared to Figure 4. In this plot, penetration is normalized by the actual length of the rod, since the penetrators were of equal mass and diameter. All the semi-infinite data, when normalized, lie on the same line. This result reflects that the greater penetration of the conical-nose-shape projectile is due to its increased length and not a direct result of nose shape.

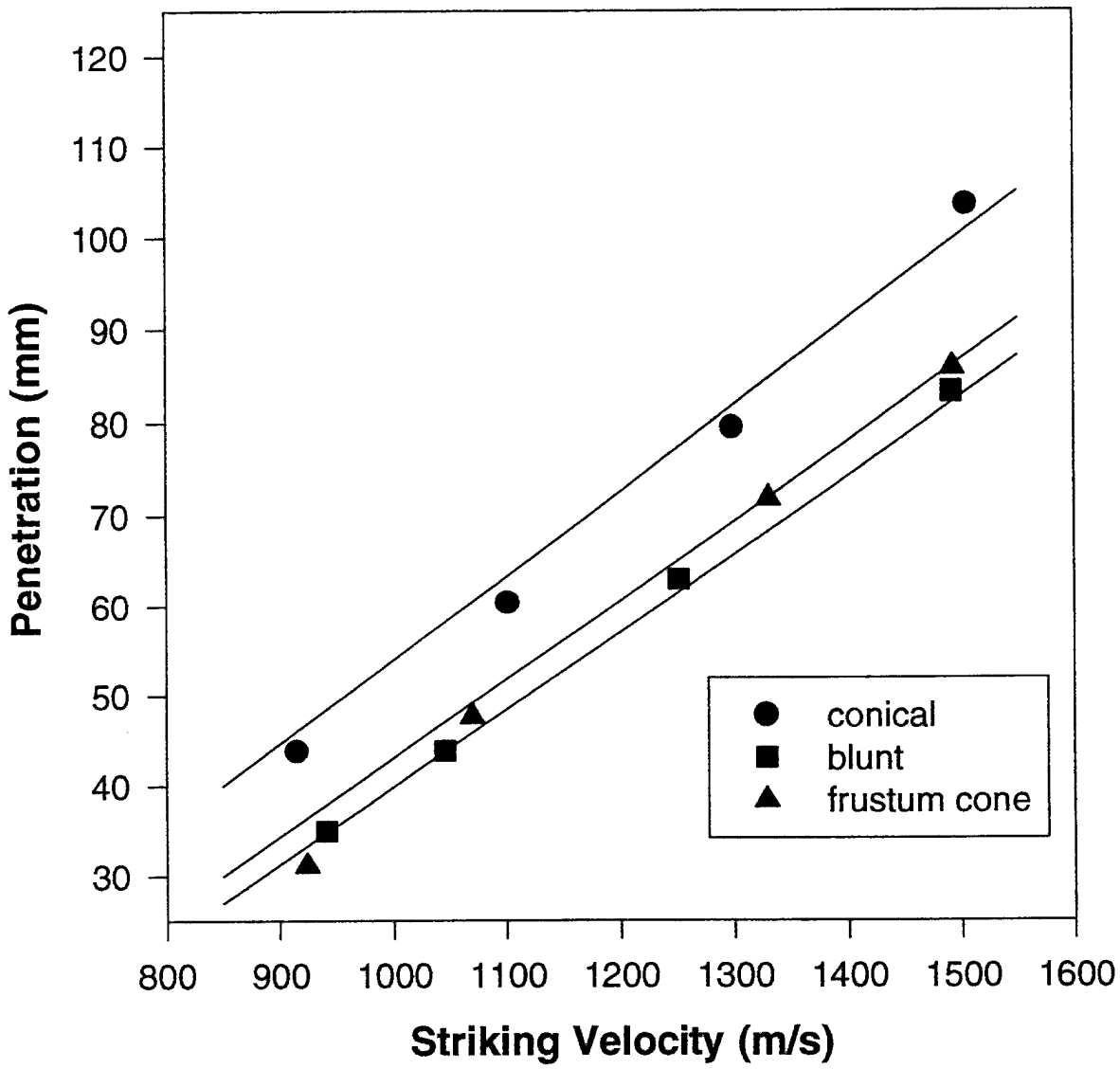

Figure 4. Plot of Semi-Infinite Penetration as a Function of Velocity.

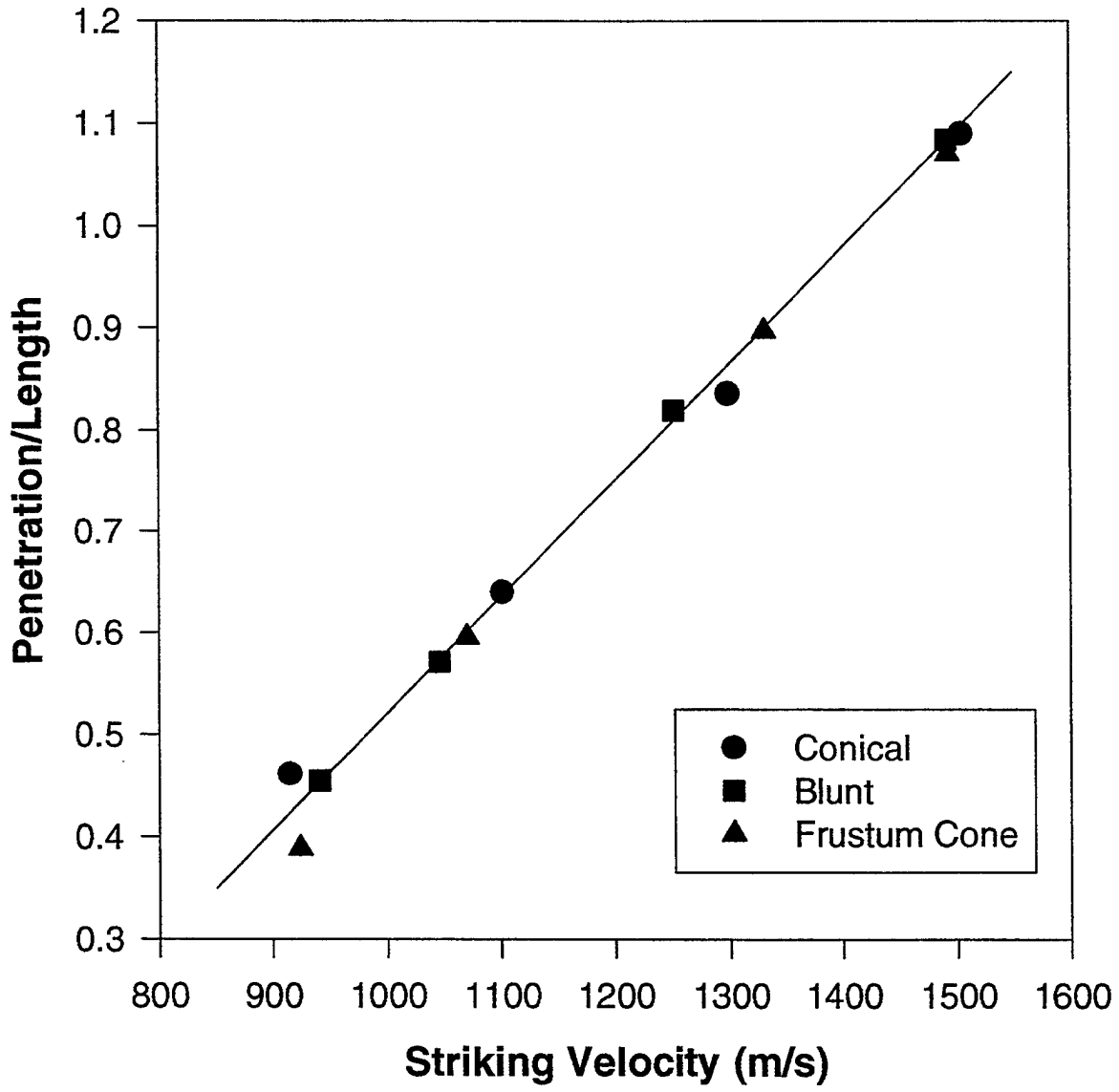

Figure 5. Plot of Normalized Penetration as a Function of Velocity.

The results of the ballistic tests with the U-3/4% Ti penetrators vs. the finite monolithic targets are listed in Table 2. For the normal-incidence, 76.2-mm RHA target, the same trend in performance observed for the semi-infinite targets is evident. The conical-nose penetrator is the best performer, delivering the lowest limit velocity of 1,239 m/s. In comparison, the limit velocities of the other nose-shape penetrators are remarkably higher at 1,324 m/s for the frustum cone and 1,373 m/s for the blunt-nose rod. An inverse ranking is seen for the high-obliquity, 70.5° target. The blunt-nose penetrator is the best performer, with a limit velocity of 1,088 m/s, and the worst performer is the conical-nose-shape design at 1,355 m/s. Once again, the performance of the frustum cone falls between the two.

The difference in the performance of the various U-3/4% Ti nose-shape penetrators is similar to the data collected previously for the WHA designs. These data points are given in Table 3 for comparison. Again, the conical-nose-shape design performed the best of the three nose-shape designs vs. the normal-incidence target with a limit velocity of 1,333 m/s and the worst against the high-obliquity target at 1,470 m/s. Similar to the U-3/4% Ti penetrators, there is a spread of approximately 120 m/s between the WHA conical- and frustum-cone-nose-shape designs against the normal-incidence finite target. In the case of the high-obliquity target, the difference in performance is approximately 275 m/s for both materials.

6. Discussion

The penetration process begins when the projectile impacts the front of the target. The nose of the rod displaces just enough target material for the remaining penetrator section to pass through. A large amount of plastic deformation occurs as the penetrator burrows into the armor. The front of the penetrator is eroded by a continuous process of building up and shearing away of the nose. As a result, the last part of the rod to be eroded is the tail. The degree of the erosion process on the projectile is determined by the material properties of the rod. The displacement of target material is caused by the moving penetrator-target interface. Finally, when the residual penetrator and the interface come to rest, the penetration process is complete, and a penetration tunnel remains.

Table 2. Limit Velocities (m/s) for U-3/4% Ti Penetrators vs. Finite RHA Targets

Nose Shape	25.4-mm RHA at 70.5°	76.2-mm RHA at 0°
Blunt	1,088	1,373
Frustum Cone	1,164	1,324
Conical	1,355	1,239

Table 3. Limit Velocities (m/s) for WHA Penetrators vs. Finite RHA Targets

Nose Shape	25.4-mm RHA at 70.5°	76.2-mm RHA at 0°
Blunt	1,186	1,440
Frustum Cone	1,246	1,415
Conical	1,470	1,333

Sectioning of the semi-infinite RHA targets revealed that the penetration channels of the three nose shapes had unique characteristics. Sketches of each penetration channel, for impacts at a velocity around 1,500 m/s, are given in Figures 6 and 7, for WHA (unpublished WHA data, Zook and Frank 1985) and U-3/4% Ti rods, respectively. For both material types, the blunt-nose-shape projectile appears to create a cavity of an almost constant diameter. In comparison, the frustum-cone-nose-shape rod creates a cavity that is slightly narrower at the entrance of the channel (the entrance hole dimensions are 16 mm × 16 mm, as compared to 21 mm × 21 mm) and then quickly widens to the uniform diameter of the blunt-nose cavity when the main body of the projectile begins to back-extrude and erode. The energy partitioning of the frustum-cone-nose-shape projectile, in terms of the penetration cavity shape, results in penetration that is slightly greater than that for the blunt-nose-shape design.

In comparison to the blunt-nose-shape projectile, the rod with a conical-nose-shape design burrows a deeper and initially narrower channel into the target at normal incidence. An examination of the sectioned target revealed a "bottleneck" or half-hourglass cavity early in the penetration process. This characteristic cavity is created by the slender nose shape entering the target. The

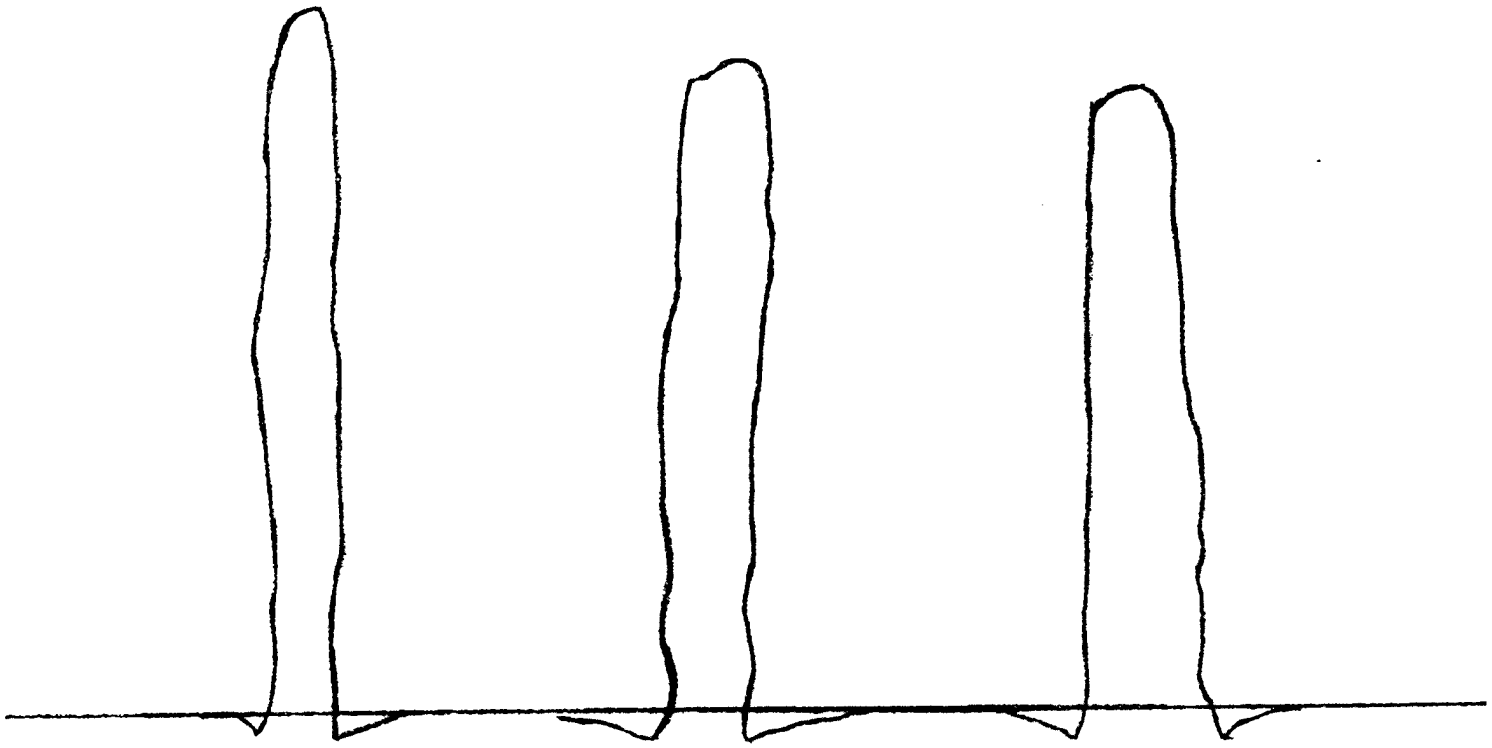

Figure 6. U-3/4% Ti Nose-Shape Projectile Semi-Infinite Penetration Channels.

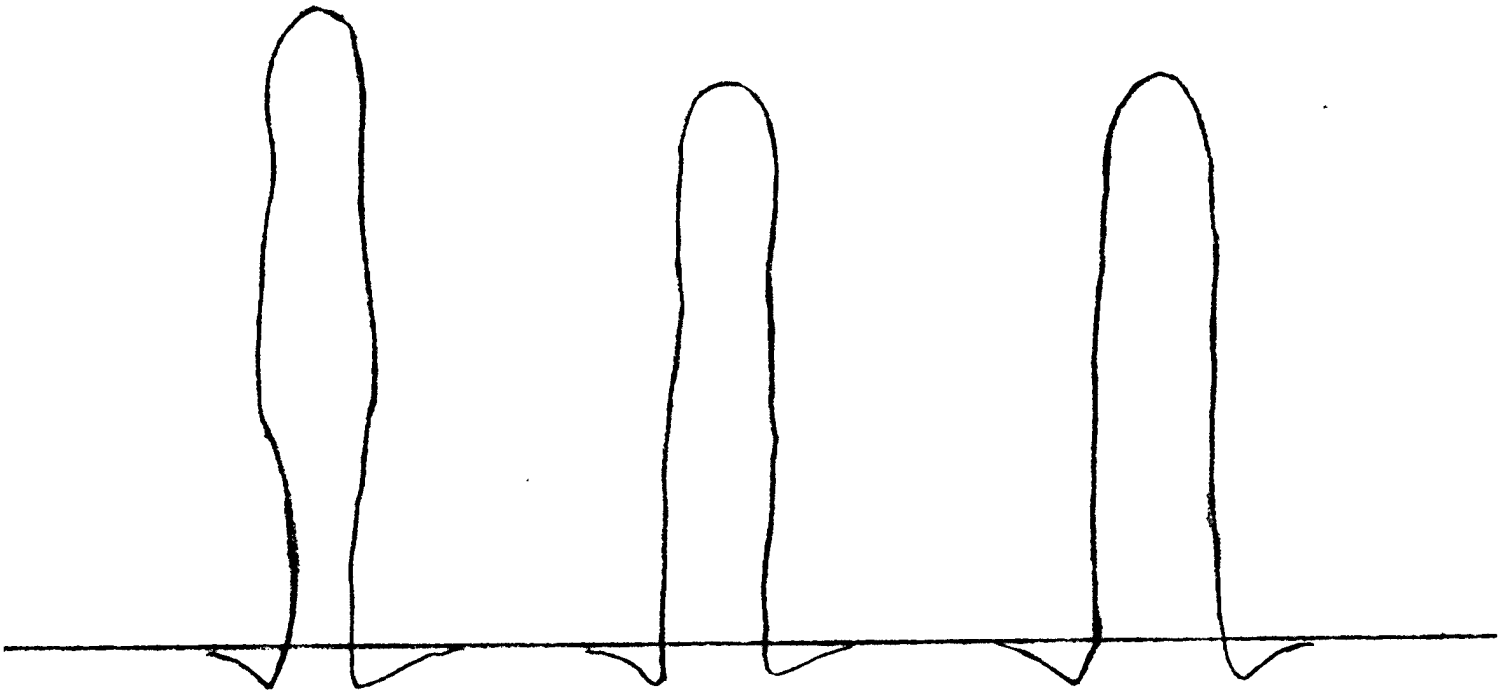

Figure 7. WHA Nose-Shape Projectile Semi-Infinite Penetration Channels.

cavity widens only as the main body of the projectile begins to penetrate. Less energy is expended to move target material away from the penetrator-target interface at the entrance area of channel. The long, conical-nose design requires that only a minimal amount of target material be displaced by the projectile as it enters the armor. The resulting entrance hole dimensions are only 11 mm × 11 mm. Later in the process, as the main body of the projectile begins to penetrate, the cavity becomes wider, consistent with projectiles of the other nose-shape designs.

Due to the way that the three nose-shape penetrators initially engage the target, there are additional differences in postmortem target measurements. The average diameter of the cavity produced by a conical-nose-shape rod at 1,500 m/s is lower at approximately 8.3 mm, whereas the average diameter displaced by the blunt-nose rod is much higher, at approximately 12.3 mm. It is evident that the early difference in the width of the penetration channel greatly influences the overall average diameter. Again, the frustum-nose-shape penetrator falls in the middle, with an average cavity diameter of 11.1 mm.

Additional differences are seen when directly comparing the performance of the WHA and U-3/4% Ti nose-shape penetrators, since the flow and failure behaviors of the two materials are fundamentally different. For U-3/4% Ti alloy penetrators, the high-pressure, high-rate loading conditions of the penetration event help the thermal softening of the penetrator material to overcome the strengthening mechanisms of deformation, such as strain hardening and strain-rate hardening. Once the penetrator softens rather than strengthens with strain, the deformation rapidly localizes as adiabatic shear bands, allowing for a quick discard of penetrator material, or chiseled nose appearance. Conventional WHAs do not flow-soften as quickly as U-3/4% Ti, and plastic localizations form only after undergoing a very large amount of plastic strain. As a result, the WHAs develop large mushroomed heads at the penetrator-target interface.

Traditionally, U-3/4% Ti projectiles outperform similar WHA projectiles. Since the eroding material is discarded earlier, and a large mushroomed head is not formed on the penetrating U-3/4% Ti rod, the volume of target material that must be displaced by the moving penetrator-target interface is minimized. Therefore, the KE is expended to displace a narrower, yet deeper, tunnel in the target.

This effect is also seen in all the nose-shape tests and is graphically represented in Figure 8, which overlays the penetration channels of the two materials. The penetration channels of the U-3/4% Ti penetrators are more narrow than the WHA penetrator channels.

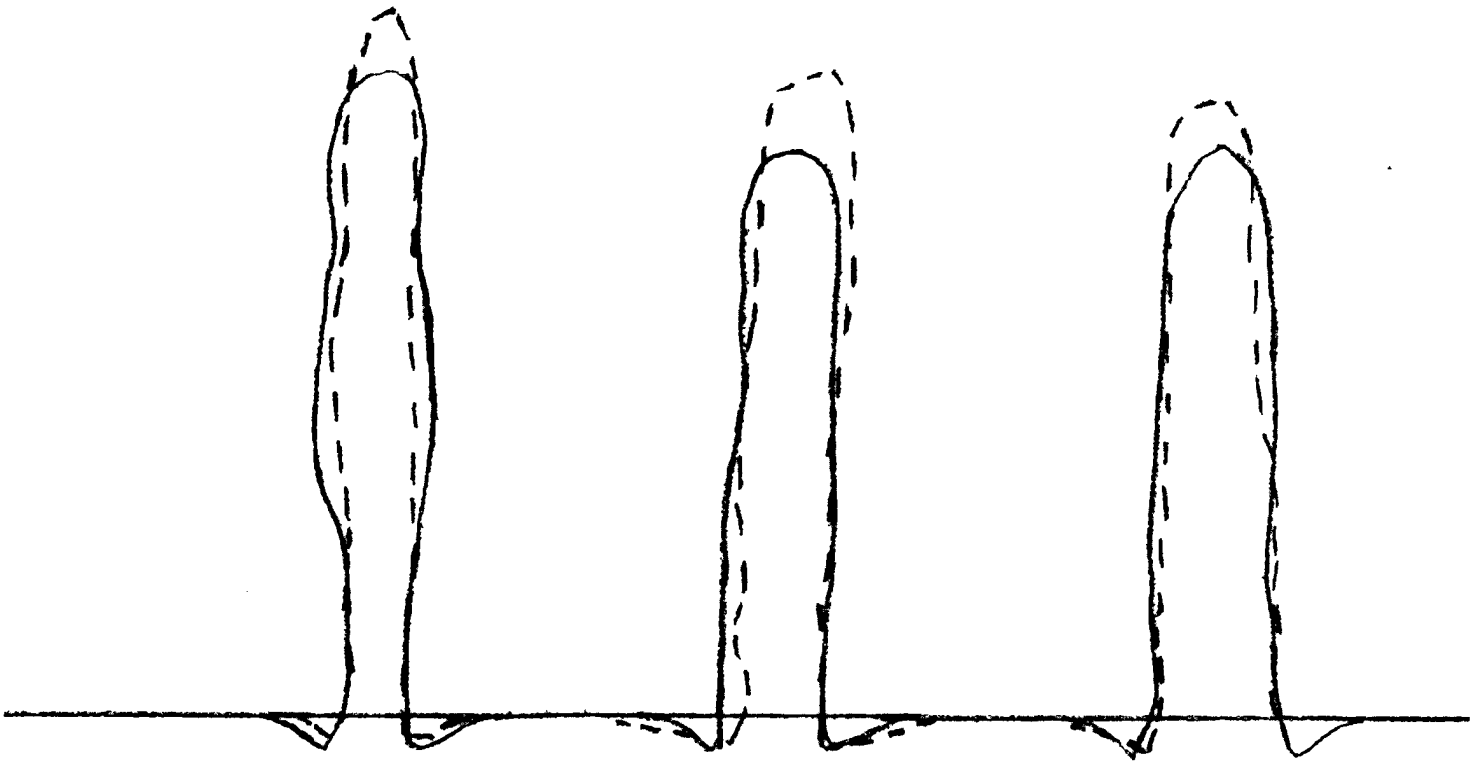

Key: - - - - - = DU

⊃ = WHA

Figure 8. Overlay of U-3/4% Ti and WHA Nose-Shape Penetration Channels.

For finite plate targets, there is a well-reported difference in limit velocity between U-3/4% Ti and WHA penetrators (Magness and Farrand 1990). This effect is also seen in these tests, resulting in a consistent shift of approximately 100 m/s in the limit velocities of WHA and depleted uranium (DU) materials. The generalized ranking of nose-shape performance is also preserved for the two

materials. The similar shifts in performances against finite and semi-infinite target imply that the nose-shape effects witnessed are independent of penetrator material.

For targets presented at obliquity, the difference in limit velocities between the blunt- and conical-nose-shape WHA penetrators was 107 m/s. A similar shift in performance, 134 m/s, was found for the U-3/4% Ti nose-shape penetrators. The consistency in the shifts between the two materials show that the early initation of shear in the U-3/4% Ti penetrators does not reduce the loss of performance at obliquity.

Nose shape is an important aspect in the overall systems approach when designing a projectile. A projectile with a conical-nose-shape design exhibits less drag resistance and reduced velocity decay in flight. Therefore, the projectile impacts the target with a greater striking velocity and has a greater available energy to defeat the target. The conical-nose-shape design on a projectile, although important to the reduction of aerodynamic drag, is also a serious liability in the defeat of an oblique target, as seen in the data results presented. This is extremely important, since most of the targets impacted by projectiles in the field are presented at obliquity. Instead of quickly embedding into the face of the target, the conical-nose-shape penetrator has the tendency to deflect against high-obliquity targets.

One approach that has been recommended in the past to combine the advantages of a conical-nose-shape design for aerodynamics and penetration performance vs. normal-incidence targets and the advantages of a more blunt-nose design vs. higher obliquity targets is to add a notch on the conical-nose-shape design (Farrand, Magness, and Leonard 1991). This design allows the nose tip to enhance normal-incidence penetration and also decrease drag resistance. When impacting high-obliquity targets, the notch provides a sacrificial section that is designed to quickly break off with only a negligible loss in penetrator mass. Tests are necessary, of course, to optimize the placement of the notch.

Another method to combine the advantages from the various nose shapes is to use a low-density (low weight), conical-shaped windscreen over a blunt-nose penetrator. The conical windscreen helps

aerodynamically (with minimal effect on terminal ballistic performance), and the blunt-nose penetrator will perform better ballistically against high-obliquity targets.

7. Conclusions

The ranking of performance of the various nose-shape U-3/4% Ti projectiles is the same as the ranking of WHA rods tested previously by Zook. Against the finite normal-incidence target, 76.2-mm RHA at 0° obliquity, the conical-nose projectile is the best performer, delivering the lowest limit velocity. The long conical nose easily engages the face of a low-obliquity target and displaces the least amount of target material. However, against a high-obliquity target, the conical-nose projectile proved to be the worst performer. Instead of readily digging into the face of the target, the conical-nose-shape design has a greater tendency to ricochet off the face of the target.

The performance of the blunt-nose penetrator acts inversely to that of the conical-nose penetrator. For both penetrator materials, it performs best against high-obliquity targets and performs the worst against low-obliquity targets. The performance of the short frustum cone, a compromise of the other two designs, fell between that of the other nose shapes for all the targets evaluated.

The consistency in the performance ranking of nose-shape designs and the delta between the two penetrator materials, demonstrates that the nose-shape effect is largely independent of penetrator material. The vastly different modes of failure, large plastic deformation for the WHA, and early adiabatic shear for the DU material did not change the overall performance ranking for the geometries evaluated.

The nose shape of a fielded munition must be a compromise of all aspects of ballistics, including aerodynamic qualities and terminal ballistic performance. Although the long conical-nose-shape design is ideal aeroballistically, these same features prove to be detrimental when impacting a high-obliquity target. This is extremely important because the most common target found on the battlefield will be impacted at obliquity. A reasonable choice to incorporate the advantages of each

design is to field a blunt-nose penetrator covered by a low-density, expendable conical windscreen. A second alternative is to place a notch on the front of a conical-nose projectile that will help aerodynamically and will also offer potentially greater performance against normal-incidence targets.

INTENTIONALLY LEFT BLANK.

8. References

Grabarek, C. L., and E. L. Herr. "X-Ray Multi-Flash System for Measurement of Projectile Performance at the Target." BRL-TN-1634, U.S. Army Ballistic Research Laboratory, Aberdeen Proving Ground, MD, September 1966.

Farrand, T., L. Magness, and W. Leonard. "A Terminal Ballistic Evaluation of a Nominally 0.60 Caliber, Mass-Stabilized, Dual Density, Electromagnetically Launched, Rodman Cone Projectile." BRL-MR-3895, U.S. Army Ballistic Research Laboratory, Aberdeen Proving Ground, MD, February 1991.

Lambert, J. P., and G. H. Jonas. "Toward Standardization in Terminal Ballistic Testing: Velocity Representation." BRL-MR-1852 (ADA021389), U.S. Army Ballistic Research Laboratory, Aberdeen Proving Ground, MD, January 1976.

Magness, L., and T. Farrand. "Deformation Behavior and Its Relationship to the Penetrator Performance of High Density KE Penetrator Materials." Proceeding from the 1990 Army Science Conference, Durham, NC pp. 465–479, May 1990.

Zook, J., C. Brown, and C. Grabarek. "The Penetration Performance of Tungsten Alloy L/D=10 Long Rods With Different Nose Shapes Fired at Rolled Homogenous Armor." BRL-MR-03350, U.S. Army Research laboratory, Aberdeen Proving Ground, MD,April 1984.

Zook, J., and K. Frank. "Comparative Penetration Performance Of Tungsten Alloy L/D=10 Long Rods With Different Nose Shapes Fired at Rolled Homogeneous Armor." BRL-MR-3480, U.S. Army Ballistic Research Laboratory, Aberdeen Proving Ground, MD, November 1985.

Zukas, J., T. Nicholas, H. Swift, L. Greszczuk, and D. Curran. *Impact Dynamics*. Krieger Publishing Company, Malabar, FL, 1992.

INTENTIONALLY LEFT BLANK.

Appendix A:

Explanation of Data Summary Tables

INTENTIONALLY LEFT BLANK.

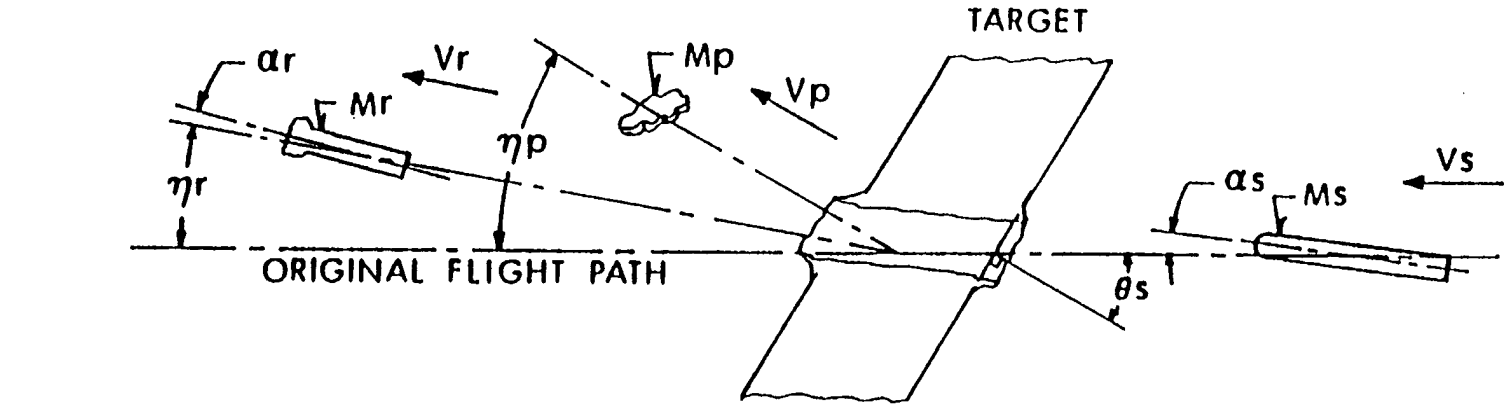

RESIDUAL PENETRATOR
Vr = VELOCITY, m/s
Mr = MASS, GRAMS
αr = INDUCED PITCH, DEGREES
ηr = INDUCED FLIGHT PATH, DEGREES

PLUG
Vp = VELOCITY, m/s
Mp = MASS, GRAMS
ηp = DEPARTURE, DEGREES

STRIKING
Vs = VELOCITY, m/s
Ms = MASS, GRAMS
αs = PITCH, DEGREES
θs = OBLIQUITY, DEGREES

Figure A-1. Primary Preimpact and Postimpact Radiographic Measures.

MEASURE	TARGET SURFACE
LENGTH (L) / WIDTH (W)	PARALLEL
HEIGHT (H) / DEPTH (D)	PERPENDICULAR

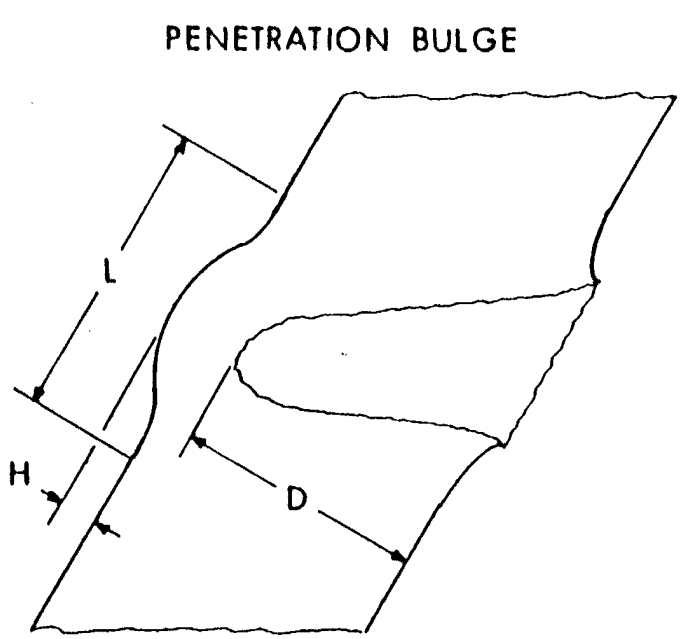

Figure A-2. Target Plate Measures: Partial Penetration.

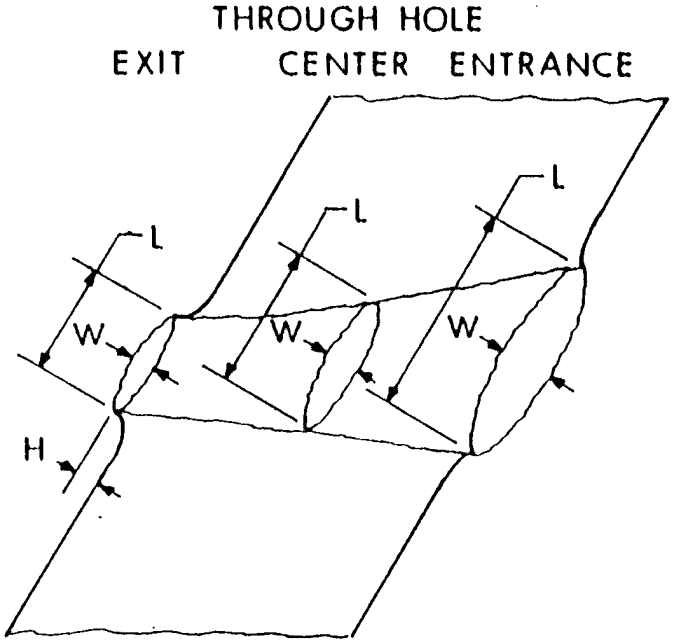

Figure A-3. Target Plate Measures: Complete Penetration.

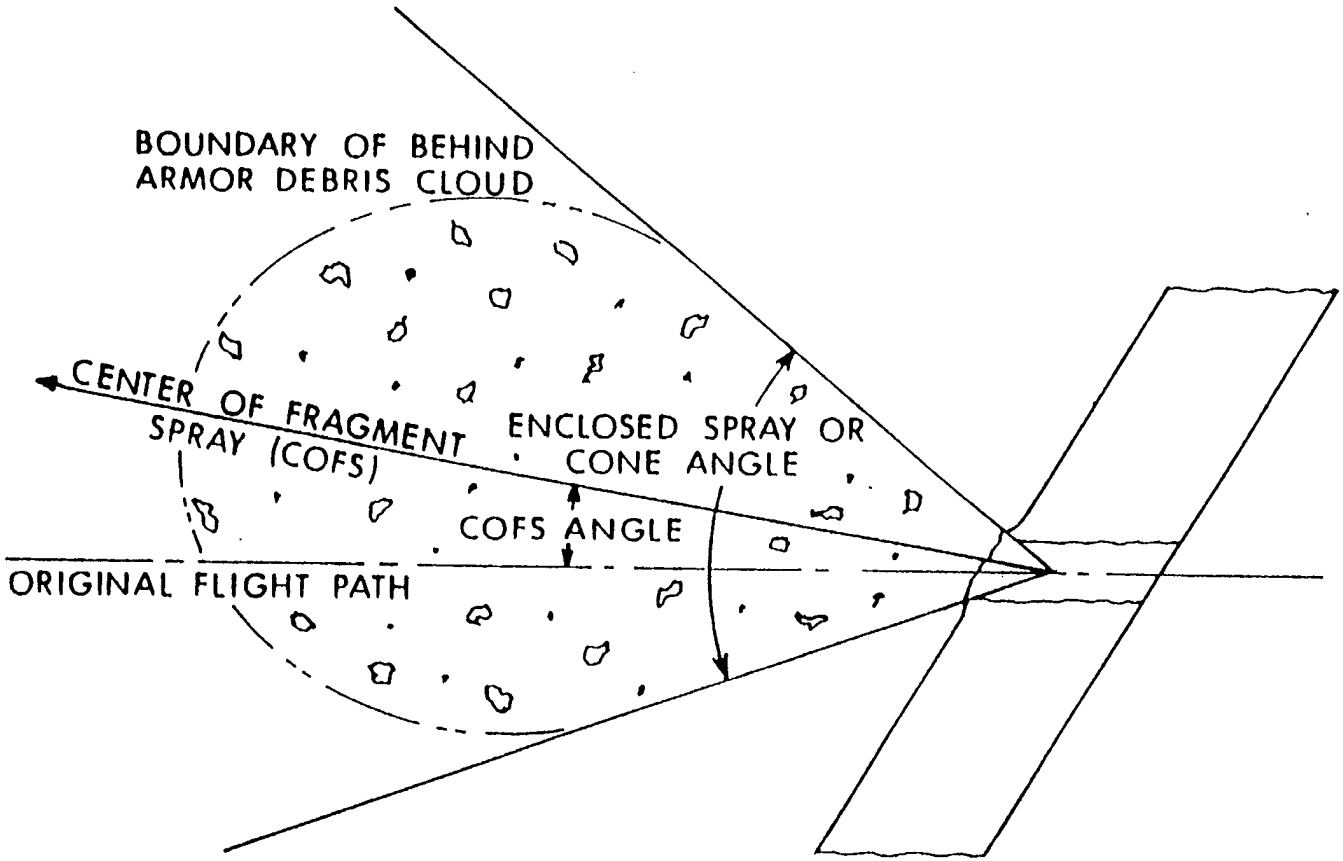

Figure A-4. Radiographic Behind-Armor Debris Measures.

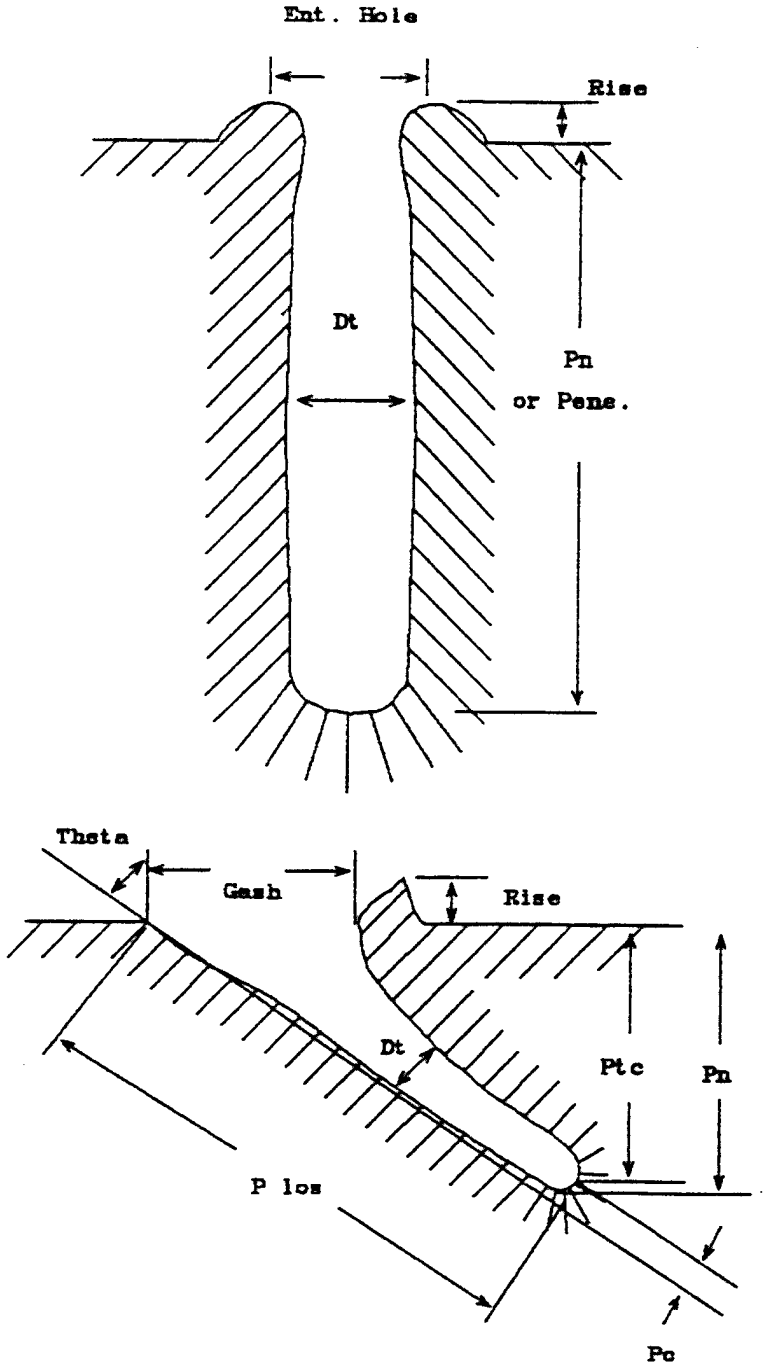

Figure A-5. Penetration Measures in Semi-Infinite Target.

Appendix B:

Data Summary Tables and Limit Velocity Curves

INTENTIONALLY LEFT BLANK.

Table B-1. Individual Shot Data for the Blunt-Nose-Shape Penetrator vs. 76.2-mm RHA at 0° Obliquity

Series Fired 1 - 1990

Sh.#	Alpha (deg)	Beta (deg)	Gamma (deg)	Vs (m/s)	Ms (g)	EtaR (deg)	AlphaR (deg)	Vr (m/s)	Mr (g)	Pen. (cm)
-4093	1.00U	1.75R	2.01	1372	66.23	NA	NA	0	0.00	6.3
4094	1.25U	1.00R	1.60	1405	66.25	0.8D	NA	293	5.54	CP
4095	0.25D	0.25R	0.34	1383	66.32	0.8D	NA	360	6.38	CP
4096	0.25D	0.25L	0.34	1368	66.30	NA	NA	0	0.00	6.6
4097	1.50U	0.50R	1.58	1378	66.33	2.0U	NA	196	4.37	CP
4098	0.50U	0.75R	0.89	1437	66.38	4.2U	NA	647	6.21	CP

Sh.#	M.rec (g)	EtaP (deg)	Vpl (m/s)	Mpl (g)	Mpr (g)	L.p (	W.p cm	Th.)	EHL (cm)	EHW (cm)	Blg (cm)	Wt.L (g)
-4093	0.00	NA	0	0.00	0.00	0.0	0.0	0.0	0.0	0.0	1.5	13
	BHN= 302											
4094	None	19.6U	164	6.63	None	0.0	0.9	0.8	1.5	1.5	NR.	7
			376	1.46	None							
	BHN= 302											
4095	None	12.1U	315	4.98	None	1.0	1.0	0.7	1.3	1.3	NR.	11
			247	0.38	None							
	BHN= 302											
4096	0.00	NA	0	0.00	0.00	0.0	0.0	0.0	0.0	0.0	1.2	4
	BHN= 302											
4097	None	16.0D	243	4.14	None	1.0	0.8	0.7	1.5	1.0	NR.	3
			91	3.69	None							
	BHN= 302											
4098	None	3.5D	684	2.33	None	0.9	0.6	0.6	2.0	2.4	NR.	17
			416	3.18	None							
	BHN= 302											

Sh.#	Cone (deg)	CoFS (deg)	EntHL (cm)	EntW (cm)	CenL (cm)	CenW (cm)	#Pcs.	M.R.Dia. (inch)	BL (cm)	BW (cm)
-4093	NA	NA	2.3	2.3	NM	NM	PP	PP	3.2	3.2
4094	51.6	6.2D	2.3	2.3	2.0	2.0	1	0.31	NM	NM
4095	19.3	2.4U	2.1	2.1	1.4	1.4	1	0.31	NM	NM
4096	NA	NA	2.0	2.0	NM	NM	PP	PP	3.0	3.0
4097	18.0	6.9D	2.2	2.2	1.8	1.8	1	0.30	NM	NM
4098	20.4	6.0D	2.1	2.0	1.5	1.5	1	0.31	NM	NM

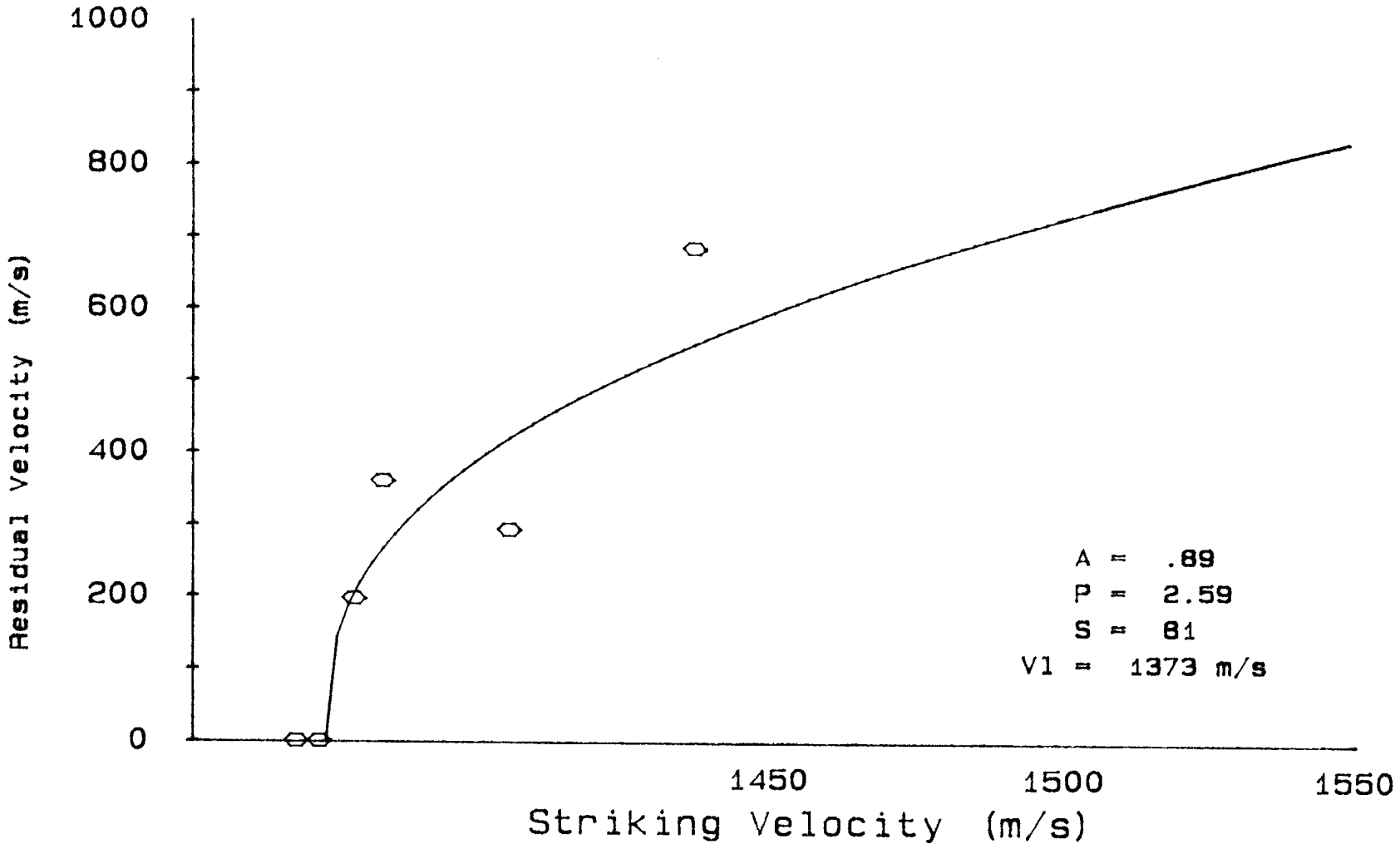

Figure B-1. Vs-Vr Curve for Blunt-Nose-Shape Penetrator vs. 76.2-mm RHA at 0° Obliquity.

Table B-2. Indivisual Shot Data for the Blunt-Nose-Shape Penetrator vs. 25.4-mm RHA at 70.5° Obliquity

Series Fired 1 - 1991

Sh.#	Alpha (deg)	Beta (deg)	Gamma (deg)	Vs (m/s)	Ms (g)	EtaR (deg)	AlphaR (deg)	Vr (m/s)	Mr (g)	Pen. (cm)
4116	0.25D	0.75R	0.79	1123	66.20	37.3U	NA	360	9.26	CP
4117	0.25D	0.50R	0.56	1108	66.29	32.6U	NA	359	7.89	CP
4118	0.25U	0.25R	0.34	1089	66.37	30.2U	NA	91	6.91	CP
4119	0.25U	0.50L	0.56	1081	66.21	NA	NA	0	0.00	3.1
4120	0.25D	0.75R	0.79	1083	66.27	NA	NA	0	0.00	2.2

Sh.#	M.rec (g)	EtaP (deg)	Vpl (m/s)	Mpl (g)	Mpr (g)	L.p (	W.p cm	Th.)	EHL (cm)	EHW (cm)	Blg (cm)	Wt.L (g)
4116	None	84.8U	116	3.62	None	1.1	0.6	0.6	2.0	1.8	NR.	16
			237	3.93	None							
	BHN= 269											
4117	None	70.6U	315	4.37	None	1.1	0.8	0.6	2.0	1.5	NR.	62
			255	4.04	None							
	BHN= 269											
4118	None	32.5U	101	0.74	None	0.5	0.5	0.4	1.4	1.3	NR.	36
			115	0.98	None							
	BHN= 269											
4119	0.00	NA	0	0.00	0.00	0.0	0.0	0.0	0.0	0.0	0.6	18
	BHN= 269											
4120	0.00	NA	0	0.00	0.00	0.0	0.0	0.0	0.0	0.0	0.5	38
	BHN= 269											

Sh.#	Cone (deg)	CoFS (deg)	EntHL (cm)	EntW (cm)	CenL (cm)	CenW (cm)	#Pcs.	M.R.Dia. (inch)	BL (cm)	BW (cm)
4116	75.4	47.1U	5.3	2.6	1.0	1.0	1	0.31	NM	NM
4117	45.8	47.7U	6.0	2.4	1.0	1.1	1	0.30	NM	NM
4118	19.5	22.8U	6.4	2.6	1.6	1.5	1	0.31	NM	NM
4119	NA	NA	6.6	2.5	NM	NM	PP	PP	5.5	3.2
4120	NA	NA	7.2	2.4	NM	NM	PP	PP	5.5	3.0

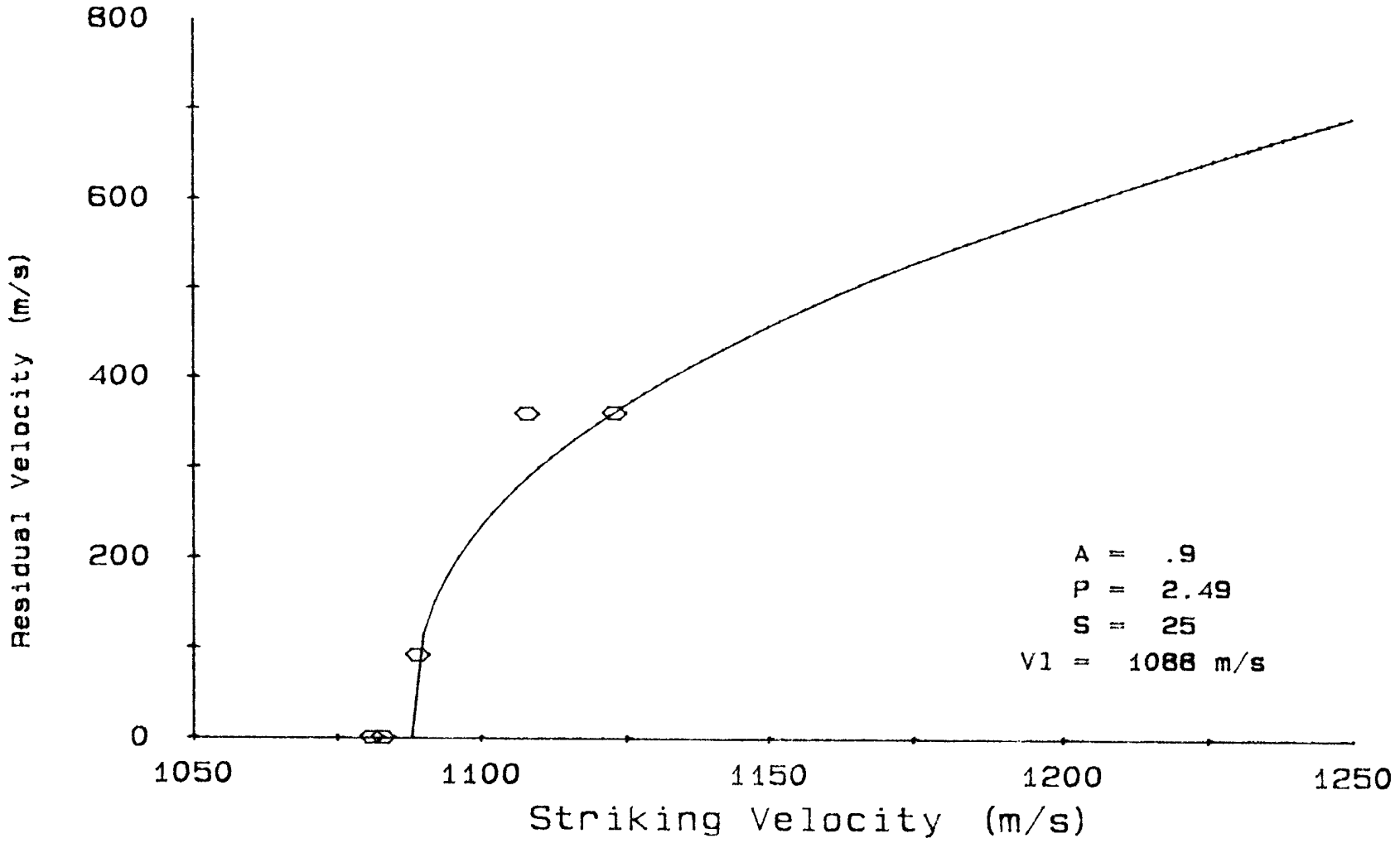

Figure B-2. Vs-Vr Curve for Blunt-Nose-Shape Penetrator vs. 25.4-mm RHA at 70.5° Obliquity.

Table B-3. Individual Shot Data for the Blunt-Nose-Shape Penetrator vs. Semi-Infinite RHA

Series Fired 1 - 1991
L/D = 10 Density is 18.6

Sh.#	Gamma (deg)	Vs (m/s)	Ms (g)	K.E. (J)	Area (scm)	M/A (g/scm)	KE/A (J/scm)	Norm P/L	Norm Pene. (mm)
4121	0.35	941	66.39	29394	0.465	143	63184	0.45	34.9
4140	1.82	1046	66.18	36204	0.465	142	77825	0.57	43.8
4143	0.90	1252	66.31	51971	0.464	143	112086	0.82	62.9
4146	1.12	1492	66.32	73816	0.464	143	159200	1.08	83.2

Sh.#	Rise (cm)	Vol base (cc)	Vol total (cc)	KE/Vt (J/cc)	KE/Vb (J/cc)	plV^2 *10^6	Dt/Dp	Area hole (scm)	M/A hole (g/scm)
4121	0.44	15.56	18.03	1630	1889	126	1.51	1.06	62.82
	BHN= 255								
4140	0.57	13.35	14.30	2532	2712	156	1.40	0.92	72.24
	BHN= 255								
4143	0.32	7.99	8.44	6158	6504	224	1.63	1.23	54.03
	BHN= 255								
4146	0.44	22.22	25.95	2845	3322	318	1.84	1.56	42.47
	BHN= 255								

Table B-4. Individual Shot Data for the Frustum-Cone-Nose-Shape Penetrator vs. 76.2-mm RHA at 0° Obliquity

Series Fired 1 - 1991

Sh.#	Alpha (deg)	Beta (deg)	Gamma (deg)	Vs (m/s)	Ms (g)	EtaR (deg)	AlphaR (deg)	Vr (m/s)	Mr (g)	Pen. (cm)
4099	1.25D	0.50L	1.35	1322	65.86	NA	NA	0	0.00	6.4
4100	0.00	0.25R	0.25	1330	65.78	1.2D	NA	318	6.55	CP
4101	0.25D	0.50L	0.56	1344	65.79	0.3D	NA	383	7.56	CP
4102	0.25D	0.25R	0.34	1334	65.74	NA	NA	0	0.00	5.5
4103	0.50U	0.50L	0.70	1371	65.88	4.7U	NA	473	5.73	CP

Sh.#	M.rec (g)	EtaP (deg)	Vpl (m/s)	Mpl (g)	Mpr (g)	L.p (	W.p cm	Th.)	EHL (cm)	EHW (cm)	Blg (cm)	Wt.L (g)
4099	0.00	NA	0	0.00	0.00	0.0	0.0	0.0	0.0	0.0	1.3	1
	BHN= 302											
4100	None	13.6U	335	4.84	None	1.0	1.0	0.6	1.5	2.0	NR.	-34
	BHN= 302											
4101	None	1.9U	384	2.26	None	0.8	0.6	0.6	1.6	1.3	NR.	-22
			218	3.83	None							
	BHN= 302											
4102	0.00	NA	0	0.00	0.00	0.0	0.0	0.0	0.0	0.0	1.4	-13
	BHN= 302											
4103	None	7.8D	373	5.20	None	0.9	0.9	0.8	1.5	1.7	NR.	-7
			359	4.24	None							
	BHN= 302											

Sh.#	Cone (deg)	CoFS (deg)	EntHL (cm)	EntW (cm)	CenL (cm)	CenW (cm)	#Pcs.	M.R.Dia. (inch)	BL (cm)	BW (cm)
4099	NA	NA	1.5	1.5	NM	NM	PP	PP	3.2	3.2
4100	14.8	6.2U	NM	NM	NM	NM	1	0.31	NM	NM
4101	28.2	9.4D	1.3	1.3	1.0	1.0	1	0.31	NM	NM
4102	NA	NA	1.3	1.3	NM	NM	PP	PP	3.1	3.1
4103	15.8	3.2D	1.5	1.5	1.3	1.3	1	0.30	NM	NM

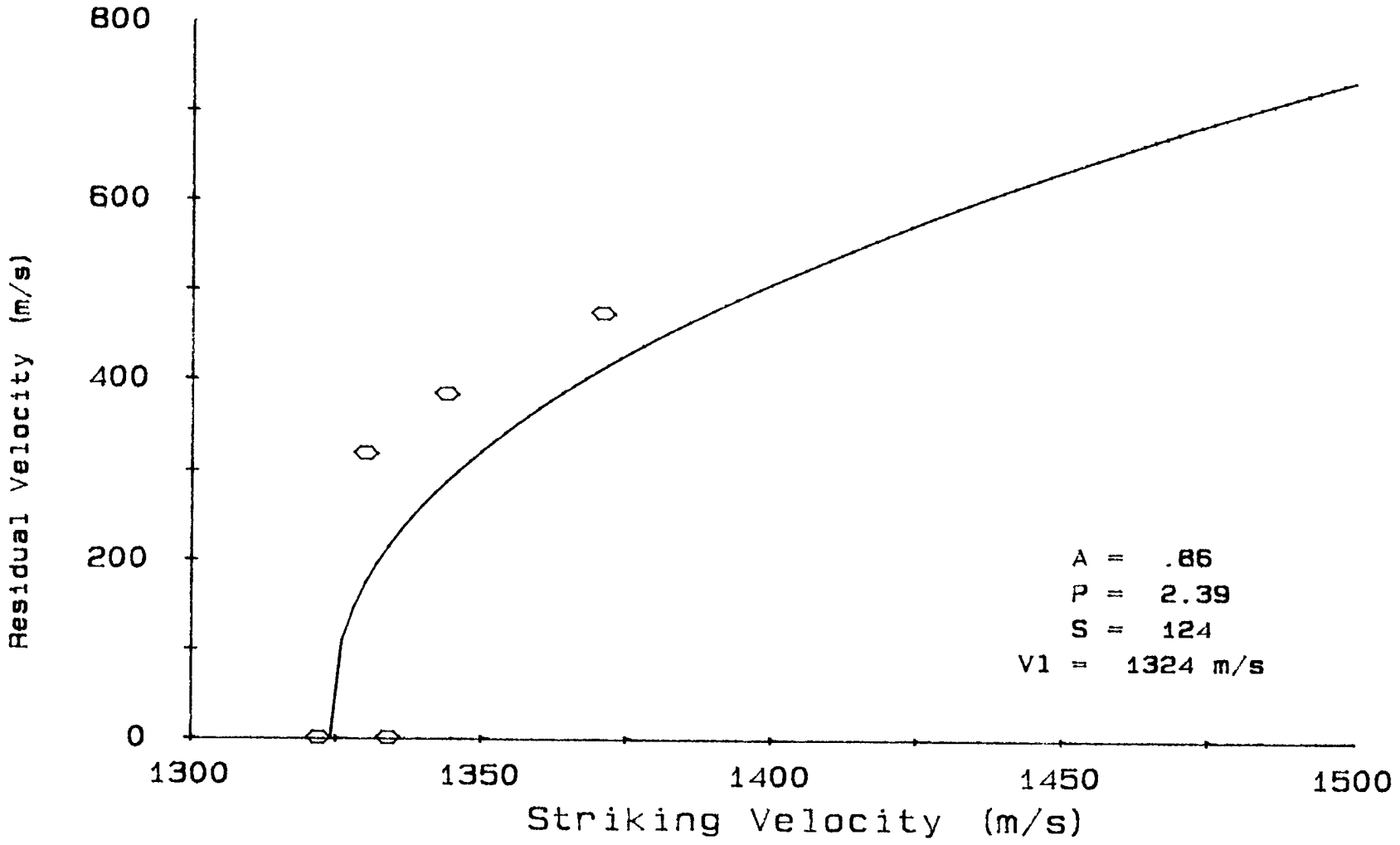

Figure B-3. Vs-Vr Curve for Frustum-Cone-Nose-Shape Penetrator vs. 76.2-mm RHA at 0° Obliquity.

Table B-5. Individual Shot Data for the Frustum-Cone-Nose-Shape Penetrator vs. 25.4-mm RHA at 70.5° Obliquity

Series Fired 1 - 1991

Sh.#	Alpha (deg)	Beta (deg)	Gamma (deg)	Vs (m/s)	Ms (g)	EtaR (deg)	AlphaR (deg)	Vr (m/s)	Mr (g)	Pen. (cm)
4104	1.00U	0.00	1.00	1285	65.75	12.8U	NA	824	10.90	CP
4122	0.50U	0.25R	0.56	1232	65.80	40.6U	NA	772	10.96	CP
4123	1.50U	0.25R	1.51	1168	65.82	25.9U	NA	536	7.39	CP
4124	0.00	0.50L	0.50	1089	65.76	NA	NA	0	0.00	0.8
4125	0.25U	0.25L	0.34	1140	65.79	NA	NA	0	0.00	2.8
4126	0.25D	0.25R	0.34	1163	65.73	NA	NA	0	0.00	1.6
4127	0.50U	1.25R	1.35	1176	65.84	NA	NA	Lost	Lost	CP
4134	0.50U	0.00	0.50	1164	66.10	NA	NA	0	0.00	1.9

Sh.#	M.rec (g)	EtaP (deg)	Vpl (m/s)	Mpl (g)	Mpr (g)	L.p (	W.p cm	Th.)	EHL (cm)	EHW (cm)	Blg (cm)	Wt.L (g)
4104	None	83.8U	180 682	7.41 2.95	None None	1.6	0.9	0.7	4.0	2.3	NR.	38
4122	BHN= 269 None	77.8U	408 214	4.51 7.95	None None	1.6	0.8	0.5	3.7	3.0	NR.	34
4123	BHN= 269 None	38.1U	356 362	1.57 3.82	None None	1.1	0.4	0.4	3.1	2.0	NR.	32
4124	BHN= 269 0.00	NA	0	0.00	0.00	0.0	0.0	0.0	0.0	0.0	0.0	16
4125	BHN= 269 0.00	NA	0	0.00	0.00	0.0	0.0	0.0	0.0	0.0	0.5	37
4126	BHN= 269 0.00	NA	0	0.00	0.00	0.0	0.0	0.0	0.0	0.0	0.3	55
4127	BHN= 269 None	Lost	Lost	Lost	None	----NM----			1.8	1.3	NR.	20
4134	BHN= 269 0.00 BHN= 269	NA	0	0.00	0.00	0.0	0.0	0.0	0.0	0.0	0.7	38

Sh.#	Cone (deg)	CoFS (deg)	EntHL (cm)	EntW (cm)	CenL (cm)	CenW (cm)	#Pcs.	M.R.Dia. (inch)	BL (cm)	BW (cm)
4104	71.3	48.5U	5.7	2.5	1.5	1.5	1	0.30	NM	NM
4122	54.6	68.0U	5.5	2.5	2.0	1.5	0	0.30	NM	NM
4123	32.1	42.0U	5.5	3.1	1.9	1.5	1	0.30	NM	NM
4124	NA	NA	7.0	2.2	NM	NM	PP	PP	0.0	0.0
4125	NA	NA	7.9	2.4	NM	NM	PP	PP	6.0	3.2
4126	NA	NA	4.5	2.2	NM	NM	PP	PP	4.5	2.2
4127	Lost	Lost	0.0	2.5	1.5	1.5	Lost	Lost	NM	NM
4134	NA	NA	7.9	2.5	NM	NM	PP	PP	5.0	3.0

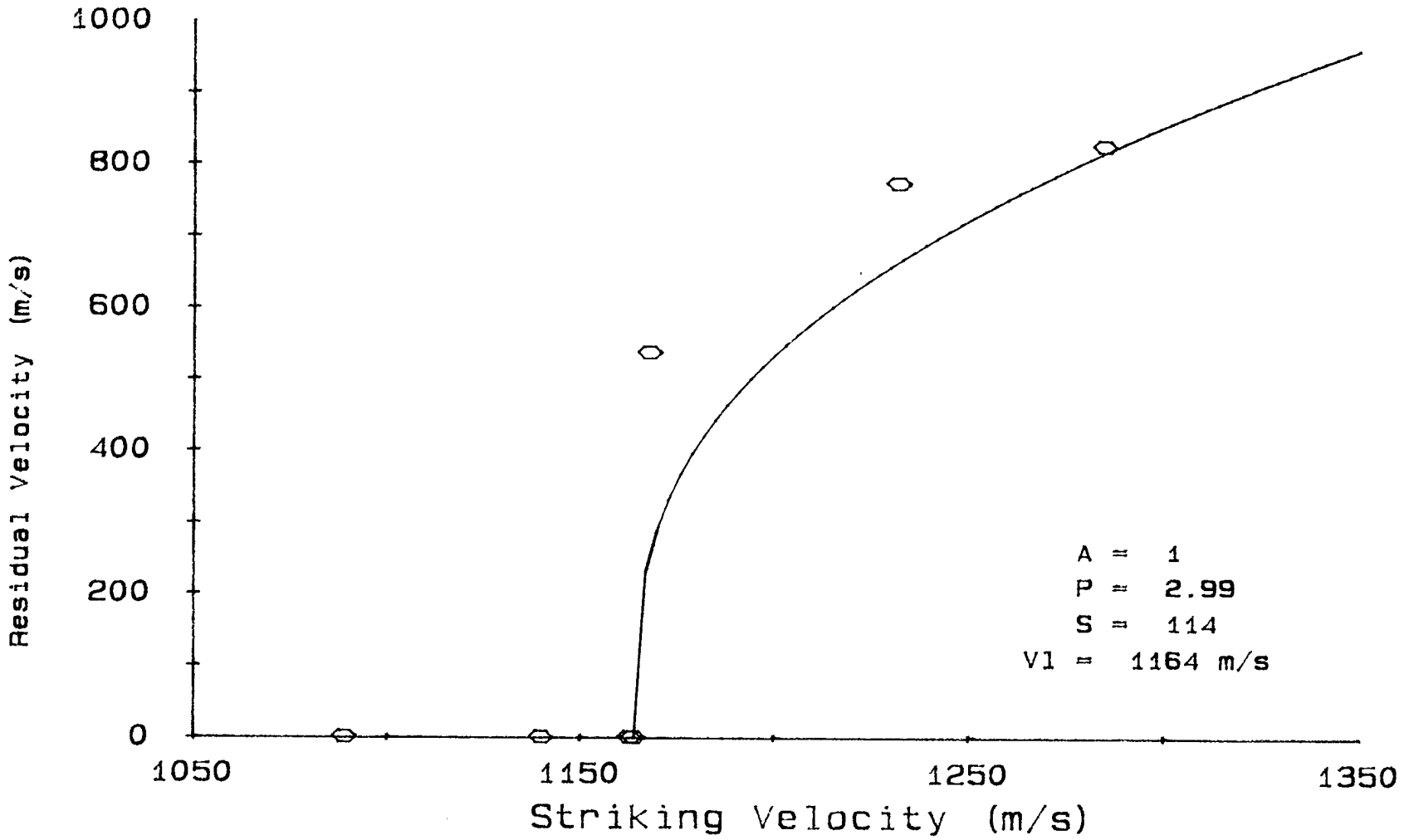

Figure B-4. Vs-Vr Curve for Frustum-Cone-Nose-Shape Penetrator vs. 25.4-m RHA at 70.5° Obliquity.

Table B-6. Individual Shot Data for the Frustrum-Cone-Nose-Shape Penetrator vs. Semi-Infinite RHA

Series Fired 1 - 1991
L/D = 10 Density is 18.6

Sh.#	Gamma (deg)	Vs (m/s)	Ms (g)	K.E. (J)	Area (scm)	M/A (g/scm)	KE/A (J/scm)	Norm P/L	Norm Pene. (mm)
4138	1.27	924	65.67	28034	0.464	142	60461	0.39	31.1
4141	0.71	1070	65.71	37616	0.464	142	81126	0.59	47.6
4144	1.03	1331	65.93	58400	0.464	142	125951	0.90	71.8
4147	0.56	1493	65.86	73403	0.464	142	158308	1.07	85.7

Sh.#	Rise (cm)	Vol base (cc)	Vol total (cc)	KE/Vt (J/cc)	KE/Vb (J/cc)	plV^2 *10^6	Dt/Dp	Area hole (scm)	M/A hole (g/scm)
4138	0.13	5.34	7.01	3999	5250	127	1.54	1.09	60.05
	BHN= 255								
4141	0.57	6.21	6.69	5623	6057	170	1.55	1.11	59.08
	BHN= 255								
4144	0.66	13.31	13.31	4388	4388	264	1.51	1.06	62.38
	BHN= 255								
4147	0.32	12.49	12.64	5807	5877	332	1.74	1.41	46.70
	BHN= 255								

Table B-7. Individual Shot Data for the Conical-Nose-Shape Penetrator vs. 76.2-m RHA at 0° Obliquity

Series Fired 1 - 1991

Sh.#	Alpha (deg)	Beta (deg)	Gamma (deg)	Vs (m/s)	Ms (g)	EtaR (deg)	AlphaR (deg)	Vr (m/s)	Mr (g)	Pen. (cm)
4105	0.25U	0.50L	0.56	1254	66.22	0.0	NA	618	10.45	CP
4106	1.25U	0.25R	1.26	1207	66.06	NA	NA	0	0.00	1.9
4107	1.00U	0.75R	1.25	1239	65.62	NA	NA	0	0.00	3.1
4108	0.50U	0.25L	0.56	1220	66.12	NA	NA	0	0.00	3.3
4109	0.00	1.75R	1.75	1271	66.01	NA	NA	0	0.00	2.0
4110	1.50U	0.50R	1.58	1288	66.05	5.3U	NA	419	7.24	CP
4111	0.75U	0.00	0.75	1265	66.03	10.7U	NA	561	9.09	CP
4112	1.00U	0.50L	1.12	1274	66.18	NA	NA	0	0.00	5.8
4113	0.75U	0.50R	0.89	1361	65.97	3.8U	NA	801	7.74	CP

Sh.#	M.rec (g)	EtaP (deg)	Vpl (m/s)	Mpl (g)	Mpr (g)	L.p (	W.p cm	Th.)	EHL (cm)	EHW (cm)	Blg (cm)	Wt.L (g)
4105	None	1.9U	637	3.54	None	1.1	0.9	0.5	2.0	1.8	NR.	6
			338	7.28	None							
	BHN= 302											
4106	0.00	NA	0	0.00	0.00	0.0	0.0	0.0	0.0	0.0	0.6	-39
	BHN= 302											
4107	0.00	NA	0	0.00	0.00	0.0	0.0	0.0	0.0	0.0	0.6	-36
	BHN= 302											
4108	0.00	NA	0	0.00	0.00	0.0	0.0	0.0	0.0	0.0	0.5	-25
	BHN= 302											
4109	0.00	NA	0	0.00	0.00	0.0	0.0	0.0	0.0	0.0	1.1	-39
	BHN= 302											
4110	None	0.0	409	2.61	None	0.8	0.7	0.6	1.3	1.3	NR.	-14
			406	2.14	None							
	BHN= 302											
4111	None	0.2U	279	2.16	None	0.8	0.6	0.6	1.3	1.8	NR.	-5
			262	1.11	None							
	BHN= 302											
4112	0.00	NA	0	0.00	0.00	0.0	0.0	0.0	0.0	0.0	0.4	-8
	BHN= 302											
4113	None	4.2D	691	2.90	None	1.1	0.7	0.5	2.5	2.2	NR.	4
			722	2.01	None							
	BHN= 302											

Table B-7. Individual Shot Data for the Conical-Nose-Shape Penetrator vs. 76.2-m RHA at 0° Obliquity (continued)

Sh.#	Cone (deg)	CoFS (deg)	EntHL (cm)	EntW (cm)	CenL (cm)	CenW (cm)	#Pcs.	M.R.Dia. (inch)	BL (cm)	BW (cm)
4105	43.1	12.3U	1.5	1.5	1.3	1.3	1	0.31	NM	NM
4106	NA	NA	1.2	1.2	NM	NM	PP	PP	3.5	3.5
4107	NA	NA	1.1	1.2	NM	NM	PP	PP	3.0	3.0
4108	NA	NA	1.0	1.0	NM	NM	PP	PP	3.5	3.5
4109	NA	NA	1.2	1.2	NM	NM	PP	PP	3.5	3.5
4110	8.3	1.2U	1.2	1.0	0.9	1.0	1	0.30	NM	NM
4111	33.5	17.0U	1.2	1.2	1.0	1.0	1	0.30	NM	NM
4112	NA	NA	1.2	1.2	NM	NM	PP	PP	3.2	3.2
4113	8.1	NM	1.1	1.1	1.0	1.0	1	0.30	NM	NM

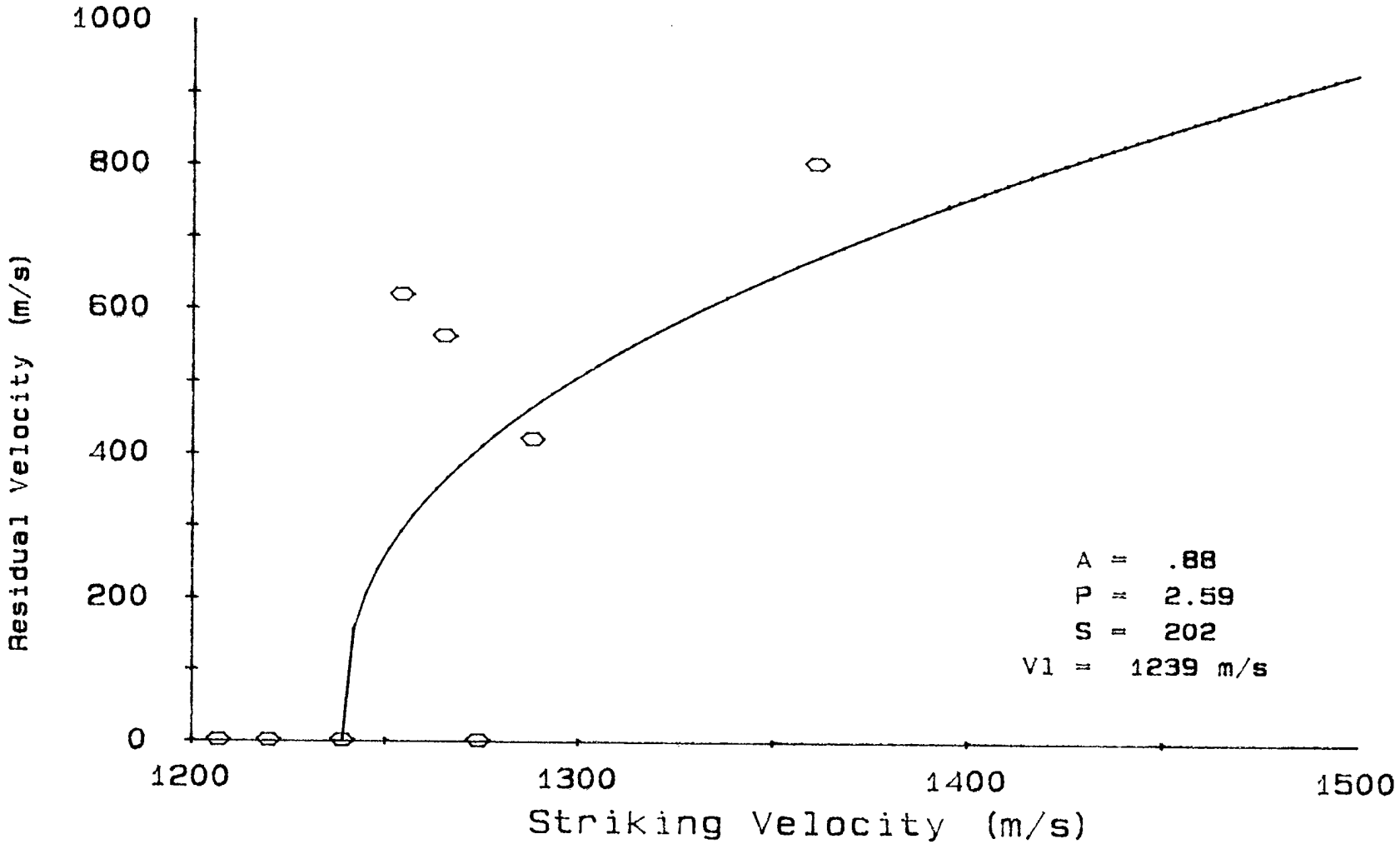

Figure B-5. Vs-Vr Curve for Conical-Nose-Shape Penetrator vs. 76.2-m RHA at 0° Obliquity.

Table B-8. Individual Shot Data for the Conical-Nose-Shape Penetrator vs. 25.4-m RHA at 70.5° Obliquity

Series Fired 1 - 1991

Sh.#	Alpha (deg)	Beta (deg)	Gamma (deg)	Vs (m/s)	Ms (g)	EtaR (deg)	AlphaR (deg)	Vr (m/s)	Mr (g)	Pen. (cm)
4128	0.50D	0.25L	0.56	1144	66.15	NA	NA	0	0.00	1.0
4129	0.00	1.00R	1.00	1196	65.96	NA	NA	0	0.00	0.8
4130	0.25D	1.25R	1.26	1214	66.10	NA	NA	0	0.00	1.1
4131	0.25U	0.75R	0.79	1327	66.06	NA	NA	0	0.00	1.5
4132	0.50U	0.75R	0.89	1384	66.23	6.3U	NA	1046	15.80	CP
4133	0.00	0.50R	0.50	1343	65.92	NA	NA	0	0.00	1.9
4135	0.25D	0.50L	0.56	1370	66.10	14.8U	NA	655	6.40	CP
4136	0.25U	0.25L	0.34	1353	66.08	NA	NA	0	0.00	2.0
4137	0.25U	0.25R	0.34	1365	66.08	NA	NA	Lost	10.10	CP

Sh.#	M.rec (g)	EtaP (deg)	Vpl (m/s)	Mpl (g)	Mpr (g)	L.p (	W.p cm	Th.)	EHL (cm)	EHW (cm)	Blg (cm)	Wt.L (g)
4128	0.00	NA	0	0.00	0.00	0.0	0.0	0.0	0.0	0.0	0.0	26
	BHN= 269											
4129	0.00	NA	0	0.00	0.00	0.0	0.0	0.0	0.0	0.0	0.0	26
	BHN= 269											
4130	0.00	NA	0	0.00	0.00	0.0	0.0	0.0	0.0	0.0	0.0	37
	BHN= 269											
4131	0.00	NA	0	0.00	0.00	0.0	0.0	0.0	0.0	0.0	0.2	83
	BHN= 269											
4132	None	17.6U	508	5.58	None	1.3	0.8	0.7	3.7	3.4	NR.	38
			396	2.75	None							
	BHN= 269											
4133	0.00	NA	0	0.00	0.00	0.0	0.0	0.0	0.0	0.0	0.2	56
	BHN= 269											
4135	None	34.9U	603	5.76	None	1.3	0.9	0.7	5.8	3.7	NR.	30
			455	1.68	None							
	BHN= 269											
4136	0.00	NA	0	0.00	0.00	0.0	0.0	0.0	0.0	0.0	0.9	21
	BHN= 269											
4137	None	Lost	442	8.83	None	1.6	1.0	0.7	3.7	2.8	0.0	50
	BHN= 269											

Table B-8. Individual Shot Data for the Conical-Nose-Shape Penetrator vs. 25.4-mm RHA at 70.5° Obliquity (continued)

Sh.#	Cone (deg)	CoFS (deg)	EntHL (cm)	EntW (cm)	CenL (cm)	CenW (cm)	#Pcs.	M.R.Dia. (inch)	BL (cm)	BW (cm)
4128	NA	NA	6.0	2.0	NM	NM	PP	PP	0.0	0.0
4129	NA	NA	7.2	2.2	NM	NM	PP	PP	0.0	0.0
4130	NA	NA	10.1	2.8	NM	NM	PP	PP	0.0	0.0
4131	NA	NA	10.9	3.0	NM	NM	PP	PP	7.0	2.0
4132	11.3	12.0U	6.5	2.8	2.5	1.5	1	0.31	NM	NM
4133	NA	NA	10.2	2.8	NM	NM	PP	PP	6.5	3.0
4135	20.2	24.9U	6.5	2.5	2.2	1.8	1	0.30	NM	NM
4136	NA	NA	7.5	2.6	NM	NM	PP	PP	8.5	2.5
4137	Lost	Lost	6.0	2.8	2.0	1.5	Lost	Lost	0.0	0.0

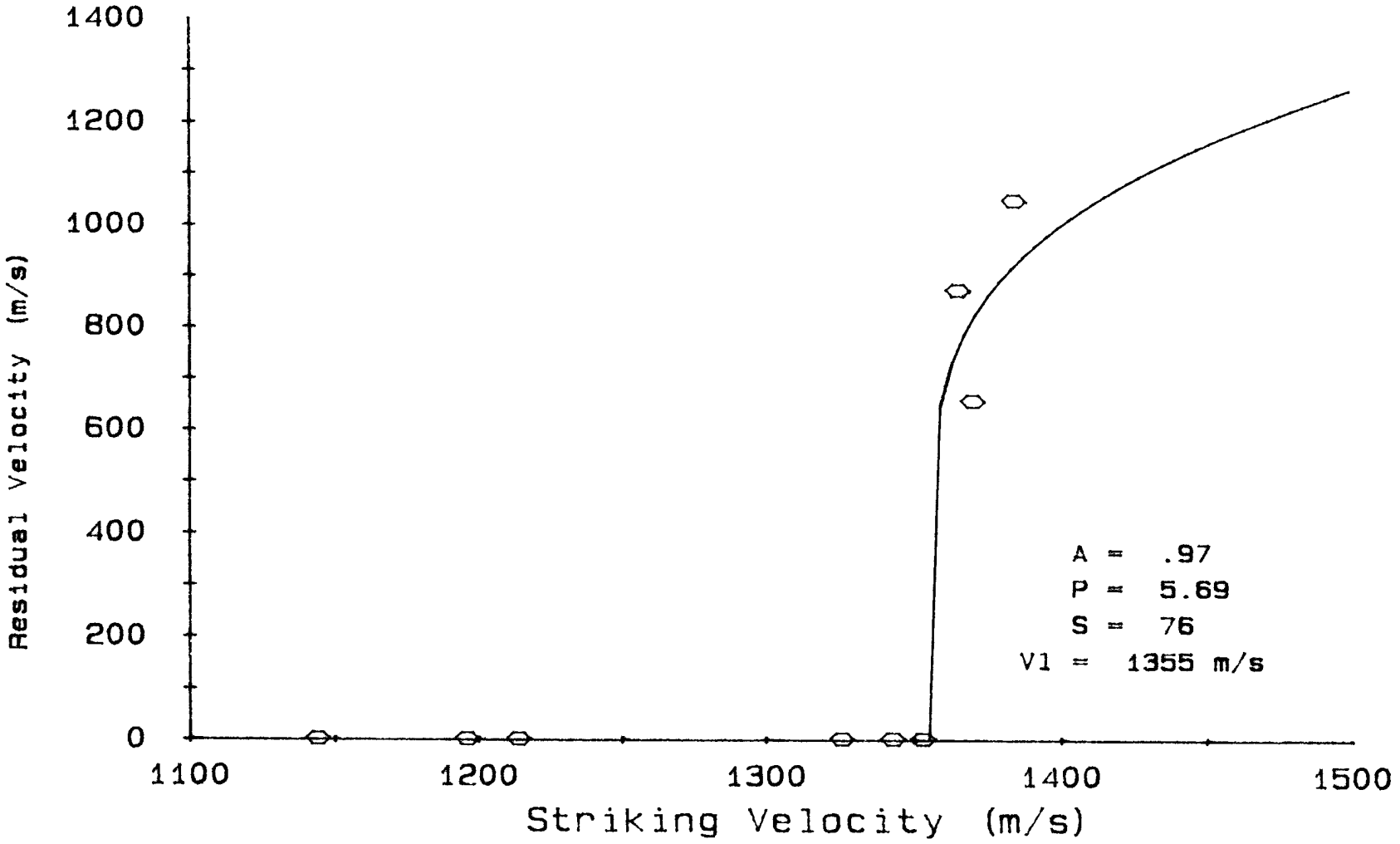

Figure B-6. Vs-Vr Curve for Conical-Nose-Shape Penetrator vs. 25.4-m at 70.5° Obliquity.

Table B-9. Individual Shot Data for the Conical-Nose-Shape Penetrator vs. Semi-infinite RHA

Series Fired 1 - 1991
L/D = 10 Density is 18.6

Sh.#	Gamma (deg)	Vs (m/s)	Ms (g)	K.E. (J)	Area (scm)	M/A (g/scm)	KE/A (J/scm)	Norm P/L	Norm Pene. (mm)
4139	1.03	915	66.10	27670	0.465	142	59480	0.46	43.8
-4142	3.81	1087	66.20	39110	0.465	142	84071	0.45	42.5
4145	0.25	1299	66.14	55802	0.465	142	119953	0.84	79.4
4148	1.25	1505	66.17	74938	0.465	142	161087	1.09	103.5
4149	0.50	1101	66.16	40100	0.465	142	86198	0.63	60.3

Sh.#	Rise (cm)	Vol base (cc)	Vol total (cc)	KE/Vt (J/cc)	KE/Vb (J/cc)	plV^2 *10^6	Dt/Dp	Area hole (scm)	M/A hole (g/scm)
4139	0.13	5.47	6.21	4456	5059	148	1.42	0.93	70.84
	BHN= 255								
-4142	0.19	10.30	13.20	2963	3797	209	1.75	1.43	46.25
	BHN= 255								
4145	0.13	8.11	9.35	5968	6881	298	1.38	0.88	74.95
	BHN= 255								
4148	0.06	16.48	16.48	4547	4547	400	1.53	1.09	60.51
	BHN= 269								
4149	0.06	7.23	7.23	5546	5546	214	1.48	1.02	64.82
	BHN= 269								

INTENTIONALLY LEFT BLANK.

NO. OF COPIES	ORGANIZATION
2	DEFENSE TECHNICAL INFORMATION CENTER DTIC DDA 8725 JOHN J KINGMAN RD STE 0944 FT BELVOIR VA 22060-6218
1	HQDA DAMO FDQ DENNIS SCHMIDT 400 ARMY PENTAGON WASHINGTON DC 20310-0460
1	CECOM SP & TRRSTRL COMMCTN DIV AMSEL RD ST MC M H SOICHER FT MONMOUTH NJ 07703-5203
1	PRIN DPTY FOR TCHNLGY HQ US ARMY MATCOM AMCDCG T M FISETTE 5001 EISENHOWER AVE ALEXANDRIA VA 22333-0001
1	PRIN DPTY FOR ACQUSTN HQS US ARMY MATCOM AMCDCG A D ADAMS 5001 EISENHOWER AVE ALEXANDRIA VA 22333-0001
1	DPTY CG FOR RDE HQS US ARMY MATCOM AMCRD BG BEAUCHAMP 5001 EISENHOWER AVE ALEXANDRIA VA 22333-0001
1	DPTY ASSIST SCY FOR R&T SARD TT T KILLION THE PENTAGON WASHINGTON DC 20310-0103
1	OSD OUSD(A&T)/ODDDR&E(R) J LUPO THE PENTAGON WASHINGTON DC 20301-7100

NO. OF COPIES	ORGANIZATION
1	INST FOR ADVNCD TCHNLGY THE UNIV OF TEXAS AT AUSTIN PO BOX 202797 AUSTIN TX 78720-2797
1	DUSD SPACE 1E765 J G MCNEFF 3900 DEFENSE PENTAGON WASHINGTON DC 20301-3900
1	USAASA MOAS AI W PARRON 9325 GUNSTON RD STE N319 FT BELVOIR VA 22060-5582
1	CECOM PM GPS COL S YOUNG FT MONMOUTH NJ 07703
1	GPS JOINT PROG OFC DIR COL J CLAY 2435 VELA WAY STE 1613 LOS ANGELES AFB CA 90245-5500
1	ELECTRONIC SYS DIV DIR CECOM RDEC J NIEMELA FT MONMOUTH NJ 07703
3	DARPA L STOTTS J PENNELLA B KASPAR 3701 N FAIRFAX DR ARLINGTON VA 22203-1714
1	SPCL ASST TO WING CMNDR 50SW/CCX CAPT P H BERNSTEIN 300 O'MALLEY AVE STE 20 FALCON AFB CO 80912-3020
1	USAF SMC/CED DMA/JPO M ISON 2435 VELA WAY STE 1613 LOS ANGELES AFB CA 90245-5500

NO. OF
COPIES ORGANIZATION

1 US MILITARY ACADEMY
MATH SCI CTR OF EXCELLENCE
DEPT OF MATHEMATICAL SCI
MDN A MAJ DON ENGEN
THAYER HALL
WEST POINT NY 10996-1786

1 DIRECTOR
US ARMY RESEARCH LAB
AMSRL CS AL TP
2800 POWDER MILL RD
ADELPHI MD 20783-1145

1 DIRECTOR
US ARMY RESEARCH LAB
AMSRL CS AL TA
2800 POWDER MILL RD
ADELPHI MD 20783-1145

3 DIRECTOR
US ARMY RESEARCH LAB
AMSRL CI LL
2800 POWDER MILL RD
ADELPHI MD 20783-1145

ABERDEEN PROVING GROUND

3 DIR USARL
AMSRL CI LP (305)

NO. OF COPIES	ORGANIZATION
1	COMMANDER US ARMY ARDEC G FLEMING PICATINNY ARSENAL NJ 07806-5000
3	COMMANDER US ARDEC AMSTA AR CCH A R CARR BLDG 354 D VO BLDG 65 S MUSALLI BLDG 65 PICATINNY ARSENAL NJ 07806-5000
1	COMMANDER US ARDEC AFAE ASM TMA MS B KOWALSKI BLDG 354 PICATINNY ARSENAL NJ 07806-5000
1	SOUTHWEST RSRCH INSTITUTE C ANDERSON J LANKFORD PO DRAWER 28510 SAN ANTONIO TX 78228-0510
1	INSTITUTE FOR ADVANCED TECH UNIVERSITY OF TEXAS AUSTIN S BLESS M NORMANDIA AUSTIN TX 78759
2	DIRECTOR LOS ALAMOS NATIONAL LAB P DUNN B HOGAN P O BOX 1663 G 770 LOS ALAMOS NM 87545
1	BRIGS CO J BACKOFEN 2668 PETER SBOROUGH ST HERDON VA 20171-2443
1	DEFENSE NUCLEAR AGENCY TECH LIB 6801 TELEGRAPH RD ALEXANDRIA VA 22192

NO. OF COPIES	ORGANIZATION
1	DIRECTOR DARPA LAND SYSTEMS OFFICE 3701 N FAIRFAX DR ARLINGTON VA 22201-1714
1	COMMANDER USA MICOM AMSMI RD W MCCORKLE REDSTONE ARSENAL AL 35898-5010
2	COMMANDER USA MICOM AMSMI RD ST WF M SCHEXNAYDER D LOVELACE REDSTONE ARSENAL AL 35898-5010
1	COMMANDER NSWC TECH LIB CHINA LAKE CA 93555
1	COMMANDER NSWC TECH LIB DAHLGREN VA 22448-5000
1	AIR FORCE WRIGHT LAB TECH LIB DR J FOSTER ARMAMENT DIVISION 101 EGLIN AVE STE 239 EGLIN AFB FL 32542
1	LANL D RABERN GROUP MEE 13 MSJ576 LOS ALAMOS NM 87545
1	LANL TECH LIB P O BOX 1663 LOS ALAMOS NM 87545

NO. OF COPIES	ORGANIZATION
3	LLNL R GOGOLEWSKI L321 R YOUNG L 282 C CLINE P O BOX 808 LIVERMORE CA 94550
2	SANDIA NATIONAL LAB A ROBINSON R NELLUMS ALBUQUERQUE NM 87185-5800
1	JOHNS HOPKINS UNIV DEPT MECH ENGINEERING K RAMESH CHARLES AND 33 ST BALTIMORE MD 21218
1	PENN STATE UNIVERSITY COLLEGE OF ENGINEERING T KRAUTHAMMER R QUNEEY R GERMAN UNIVERSITY PARK PA 16802-6809
1	KAMAN SCIENCES CORP N ARI S DIEHL 1500 GARDEN OF THE GODS RD COLORADO SPRINGS CO 80907

NO. OF COPIES	ORGANIZATION
	ABERDEEN PROVING GROUND
24	DIR USARL AMSRL WM TC T BJERKE B DEROSSET F GRACE E KENNEDY M LAMPSON R MUDD R SUMMERS W WALTERS L MAGNESS B PHILLABAUM R COATES B SORENSEN AMSRL WM TD K FRANK T FARRAND G BOYCE D DIETRECH AMSRL WM TA M KEELE W ROWE D HACKBARTH M BURKINS M ZOLTOSKI E RAPACKI N RUPERT J RUNYEON

REPORT DOCUMENTATION PAGE

Form Approved
OMB No. 0704-0188

1. AGENCY USE ONLY *(Leave blank)*	2. REPORT DATE	3. REPORT TYPE AND DATES COVERED
	September 1997	Final, Feb 90 - May 97

4. TITLE AND SUBTITLE

The Effect of Nose Shape on Depleted Uranium (DU) Long-Rod Penetrators

5. FUNDING NUMBERS

1L162618AH0

6. AUTHOR(S)

Wendy Leonard

7. PERFORMING ORGANIZATION NAME(S) AND ADDRESS(ES)

U.S. Army Research Laboratory
ATTN: AMSRL-WM-TC
Aberdeen Proving Ground, MD 21005-5066

8. PERFORMING ORGANIZATION REPORT NUMBER

ARL-TR-1505

9. SPONSORING/MONITORING AGENCY NAMES(S) AND ADDRESS(ES)

10.SPONSORING/MONITORING AGENCY REPORT NUMBER

11. SUPPLEMENTARY NOTES

12a. DISTRIBUTION/AVAILABILITY STATEMENT

Approved for public release; distribution is unlimited.

12b. DISTRIBUTION CODE

13. ABSTRACT *(Maximum 200 words)*

The ballistic perfromance of model scale U-3/4%Ti long-rod penetrators with three different nose-shape designs (blunt nose, conical nose, and frustum cone) were evaluated. The target matrix included semi-infinite rolled homogeneous armor (RHA) and two finite RHA targets, one at normal incidence and one at high obliquity, but with the same line-of-sight thickness. The results reflected the same trends as observed for a previous tungsten alloy penetrator study, demonstrating that the nose-shape effects are independent of penetrator material.

14. SUBJECT TERMS

U-3/4%Ti, terminal ballistic performance, model scale, limit velocity, nose-shape designs

15. NUMBER OF PAGES

53

16. PRICE CODE

17. SECURITY CLASSIFICATION OF REPORT	18. SECURITY CLASSIFICATION OF THIS PAGE	19. SECURITY CLASSIFICATION OF ABSTRACT	20. LIMITATION OF ABSTRACT
UNCLASSIFIED	UNCLASSIFIED	UNCLASSIFIED	UL

INTENTIONALLY LEFT BLANK.

USER EVALUATION SHEET/CHANGE OF ADDRESS

This Laboratory undertakes a continuing effort to improve the quality of the reports it publishes. Your comments/answers to the items/questions below will aid us in our efforts.

1. ARL Report Number/Author ARL-TR-1505 (Leonard) Date of Report September 1997

2. Date Report Received _____

3. Does this report satisfy a need? (Comment on purpose, related project, or other area of interest for which the report will be used.) _____

4. Specifically, how is the report being used? (Information source, design data, procedure, source of ideas, etc.) _____

5. Has the information in this report led to any quantitative savings as far as man-hours or dollars saved, operating costs avoided, or efficiencies achieved, etc? If so, please elaborate. _____

6. General Comments. What do you think should be changed to improve future reports? (Indicate changes to organization, technical content, format, etc.) _____

CURRENT ADDRESS

_____
Organization

_____
Name E-mail Name

_____
Street or P.O. Box No.

_____
City, State, Zip Code

7. If indicating a Change of Address or Address Correction, please provide the Current or Correct address above and the Old or Incorrect address below.

OLD ADDRESS

_____
Organization

_____
Name

_____
Street or P.O. Box No.

_____
City, State, Zip Code

(Remove this sheet, fold as indicated, tape closed, and mail.)

(DO NOT STAPLE)

DEPARTMENT OF THE ARMY

OFFICIAL BUSINESS

NO POSTAGE
NECESSARY
IF MAILED
IN THE
UNITED STATES

BUSINESS REPLY MAIL
FIRST CLASS PERMIT NO 0001,APG,MD

POSTAGE WILL BE PAID BY ADDRESSEE

DIRECTOR
US ARMY RESEARCH LABORATORY
ATTN AMSRL WM TC
ABERDEEN PROVING GROUND MD 21005-5066